CHAPTER–3A

Analysis of Photophysical Properties in Bis(aryl)-di-imines and Correlating with their Structural features

Analysis of Photophysical Properties in Bis(aryl)-di-imines and Correlating with their Structural features

3A.1 Introduction

Potential applications[1] of light-emitting materials include organic light-emitting diodes (OLEDs), sensors, and biological imaging, which require them to have enhanced luminescence efficiency in the aggregated state. Tang and coworkers, in 2001, first explored the aggregation-induced emission (AIE) and reported a series of tetraphenylethene derivatives.[2] Park's group[3] and Tian's group[4] have reported several material systems possessing AIE properties. The AIE behavior is rationalized by considering the restriction of intramolecular rotation, the formation of J-aggregates, and intramolecular planarization.[5]

The assembling of small molecules in solid-state can often be categorized as H-aggregates and J-aggregates. In H-aggregate, the stacking of the molecules is face-to-face, while J-aggregate results due to the head-to-tail arrangement. The formation H- and J-aggregates results in modification of the excited state energies and hence affects absorption and photoluminescence spectra. The energy diagram drawn according to Kasha's exciton theory[6] is shown in Figure 3A.1. The electronically excited state $*S_1$ splits into two exciton states $*S'_1$ and $*S''_1$ due to parallel and antiparallel transition dipole moment of adjacent molecules. From this diagram, it is clear that absorption maxima in H-aggregate is blue shifted with respect to the monomer and J-aggregate is red shifted. Generally, H-aggregates are non-emissive due to the forbidden transition and energy loses through non-radiative pathway which are represented by the sting ray arrow.

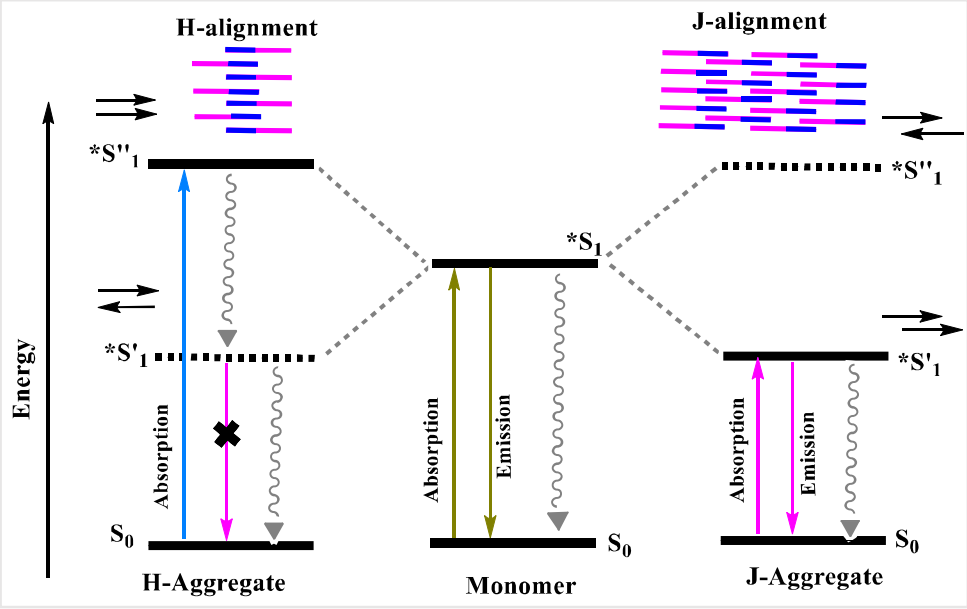

Figure 3A.1: Energy diagram for H- and J-aggregates based on Kasha's excitation theory model

The solid-state arrangement of the molecules, in general, decides the properties of a compound, and this information can be obtained by analyzing the crystal structure of that compound. The knowledge of supramolecular packing of the molecules and its relationship with the photophysical properties will pave the way to develop the strategies in designing new materials which target the light-emitting properties. Synthesis of materials by utilizing non-covalent interactions is an efficient route and a handy method to tailor light-emitting solids. Draper and coworkers have used supramolecular synthesis and tuned the solid-state luminescence of 2-cyano-3-(4-(diphenylamino)phenyl) acrylic acid by reacting them with substituted pyridines and amines.[7] Varughese has reviewed the utilization of non-covalent methods in the synthesis solid state emitting molecular materials and their applications.[8]

Compounds based on Schiff bases have been explored widely because of their easy synthetic procedures, photophysical properties, and biological activities.[9] Kawasaki et al., have studied the solid-state photoluminescence (PL) spectra of a series of salen compounds (Schiff bases) with varying alkylene chain lengths and observed the relation of the photophysical properties with alkylene chain length.[10] Xiang et al., have reported aggregation induced emission (AIE) in salicylaldehyde azine molecule, where no quenching was observed despite having planar geometry.[11] Later on, Xiang, Liu and coworkers observed a unique AIE from the non-conjugated salen compounds, where the small π-conjugated system produced AIE with large Stokes shifts and high fluorescence quantum yields.[12]

Di-imine based compounds with alkylene groups as spacer and pyridyl/aromatic moieties at extremities have been studied by various groups (Scheme 3A.1). Reports are available on the crystal structure analysis of **L1a**, **L1b,** and **L2a** along with their property studies. The absorption spectra of azines and dianils including **L1a**, **L1b**, **L2a** and **L2b** were reported by Ferguson and Goodwin in 1949.[13] Sinha has studied the crystal structure of **L1a** and reported the effect of conjugation on the bond lengths.[14] Glaser et al., have explored the solid-state structures of a series of acetophenone azines including **L1b**,[15] while the structure of **L2b** has been analyzed by the research group of Tiekink.[16] The electrochemical behavior of the acetophenone azines has been studied by Workentin et al., where the effect of substituents on the aryl group on the electrochemical potential has been evaluated.[17] Research group of Ding has observed pressure induced phase transformation in **L1a** through their high pressure spectral analysis.[18] Xiang et al., have studied the emission properties of **L1a** and observed that this compound exhibit no AIE property.[12]

Our group has previously reported the photophysical properties of bis(pyridyl)-di-imine compound (**L1c-d**, **L2c-d**, **L3c-d**) along with the structural description, where it was concluded that the flexible spacer (alkylene bridge) in these molecules helped in aggregating the molecules causing enhanced emission.[19] The absence of alkylene spacer has resulted non-existence of fluorescence property due to intramolecular rotation in lack of intermolecular H-bonding and excimer or H-aggregate dimer formation. Crystal structure analysis of di-imine molecule with **L1d** showed presence of three types of molecules with parallel alignment (Figure 3A.2). Molecules containing ethylene and 1,4-butylene spacers have shown the crystallization induced emission due to their way of packing in crystal which is controlled by the non-covalent interaction (Figure 3A.3). The structural *anti* conformations, *gauche-anti-gauche* conformation (ethylene and butylene) led to planar geometry and avoid excimer formation in solution to solid-state. Ethylene and butylene spacer containing ligands have shown enhanced emission in solid-state than in solution state.

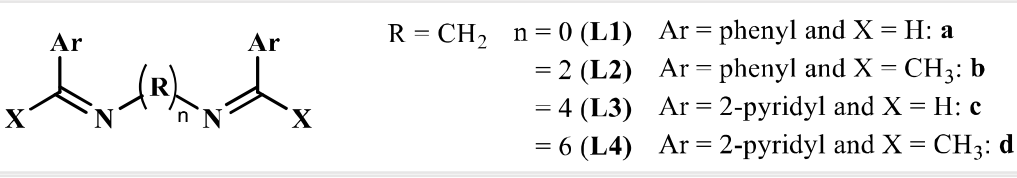

Scheme 3A.1: Bis(aryl)-di-imine ligands with $(CH_2)_n$ spacer backbone

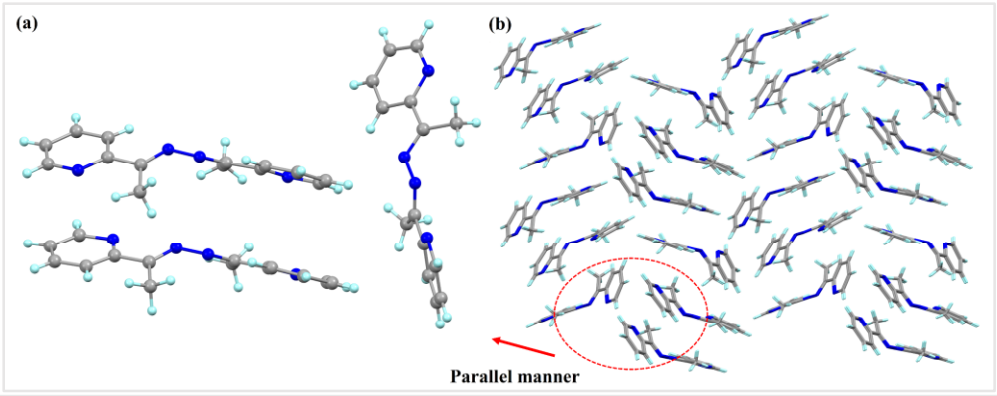

Figure 3A.2: Three types of molecule array in face-to-face stacking in **L1d**

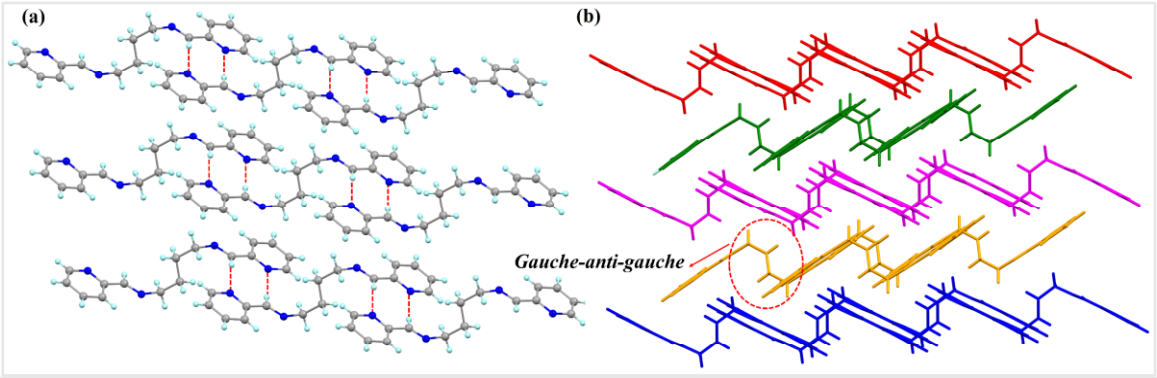

Figure 3A.3: C-H•••N interactions of butylene spacer resulted in corrugated layers of head-to-tail interaction

In this chapter, photophysical properties of bis(aryl)-di-imine molecules (Scheme 3A.1) in the solid as well as solution states is studied. The observations are rationalized on the following grounds: (i) Effect of alkylene chain length; (ii) Presence of methyl group on the methinine carbon; (iii) Comparison of the light-emitting properties with the pyridyl based Schiff base compounds.

3A.2 Experimental

3A.2.1 General

Infrared spectra were taken on ABB Bomen MB-3000 FTIR instrument. UV-Visible spectra and Fluorescence spectra were taken using Jasco V-650 and Fluorimax-4 0426C–0809 spectrophotometers, respectively. ^{1}H and ^{13}C NMR spectra were recorded on 400 MHz Bruker AVANCE III spectrometer and Powder X-Ray Diffraction (XRD) data was collected with Rigaku Miniflex II, λ =1.54, Cu Kα. Time correlated single photon count (TCSPC) instrument was used for lifetime measurements and Quanta phi was used for absolute quantum yield determination.

The compounds **L1**-**L4** were synthesized by the usual method of preparation of Schiff bases, which involved the condensation reaction of primary diamines with an aldehyde/ketone precursor in alcoholic solution under reflux conditions.

3A.2.2 Synthesis of 1,2-di((*E*)-benzylidene)hydrazine (L1a)[13]

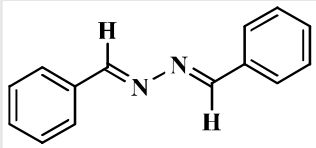

Hydrazine hydrate (0.5 mL, 10 mmol) was added drop wise to an ethanolic solution of benzaldehyde (2.0 mL, 20 mmol). The mixture was refluxed for 6 hours. The solvent was removed under vacuum and the yellow color solid product was recrystallized from methanol. Yield: 36%; Melting point: 86-87 ºC; IR (cm^{-1}, KBr pellet): 3418(w), 3171(w), 3047(w), 3001(w), 2947(m), 1666(m), 1628(vs), 1574(w), 1489(w), 1443(m), 1304(w), 1203(w), 957(m), 856(w) (Figure A-1). ^{1}H NMR (400 MHz, DMSO-d_6) δ ppm: 8.73 (2H, s, imine CH), 7.90 (4H, m, ArH), 7.51 (6H, br, ArH) (Figure A-2); ^{13}C NMR (100 MHz, DMSO-d_6) δ ppm: 161.99, 134.24, 131.84, 129.38, 128.84 (Figure A-3).

3A.2.3 Synthesis of (1*E*,2*E*)-1,2-bis(1-phenylethylidene)hydrazine (L1b)[15]

Hydrazine hydrate (0.5 mL, 10 mmol) was added dropwise to a solution of acetophenone (2.3 mL, 20 mmol) in ethanol (40 mL). The mixture was refluxed for 6 hours. The solvent was

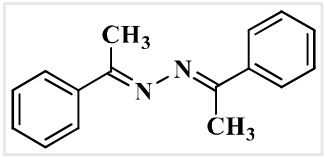

removed under vacuum and the yellow color solid product was recrystallized from methanol. Yield: 46%; Melting point: 122-123 ºC; IR (cm^{-1}, KBr pellet): 3418(m), 3055(m), 2962(m), 2916(w), 1643(vs), 1566(vs), 1489(w), 1443(vs), 1358(vs), 1281(s), 1072(m), 1018(m), 756(vs) (Figure A-4); ^{1}H NMR (400 MHz, DMSO-d_6) δ ppm: 7.92 (4H, dd, *J* = 6.6, 3.1 Hz, ArH), 7.50-7.44 (6H, br, ArH), 2.28 (6H, s, 2×CH_3) (Figure A-5); ^{13}C NMR (100 MHz, DMSO-d_6) δ ppm: 157.77, 138.77, 130.54, 128.79, 15.19 (Figure A-6).

3A.2.4 Synthesis of (1*E*,1'*E*)-*N*,*N*'-(ethane-1,2-diyl)bis(1-phenylmethanimine) (L2a)[13]

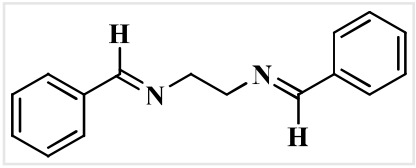

Ethylene diamine (0.7 mL, 10 mmol) was added dropwise to a solution of benzaldehyde (2.0 mL, 20 mmol) in ethanol (40 mL) and the mixture was refluxed for 6 hours. The solvent was removed under vacuum and the orange semi-solid product obtained was recrystallized from hexane. Yield: 38%; Melting point: 60-61 ºC; IR (cm^{-1}, KBr pellet): 3418(m), 3271(w), 3055(w), 3032(w), 2908(w), 2843(m), 1674(w), 1643(vs), 1574(w), 1450(m), 1373(m), 1281(w), 157(w), 1018(s), 972(w), 918(w) (Figure A-7); ^{1}H NMR (400 MHz, DMSO-d_6) δ ppm: 8.34 (2H, s, imine CH), 7.79 – 7.66 (4H, m, ArH), 7.49 – 7.36 (6H, br, ArH), 3.88 (4H, s, 2×CH_2) (Figure A-8); ^{13}C NMR (100 MHz, DMSO-d_6) δ ppm: 162.44, 136.49, 131.09, 129.11, 128.28, 61.39 (Figure A-9).

3A.2.5 Synthesis of (1*E*,1'*E*)-*N*,*N*'-(ethane-1,2-diyl)bis(1-phenylethan-1-imine) (L2b)[16]

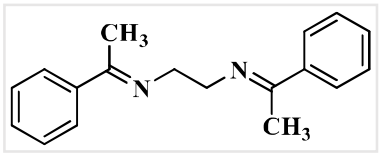

Ethylene diamine (0.7 mL, 10 mmol) was added dropwise to a solution of acetophenone (2.3 mL, 20 mmol) in ethanol (40 mL). The mixture was refluxed for 6 hours. The solvent was removed under vacuum and crude brown semi-solid product was recrystallized from hexane. Yield: 36%; Melting point: 107-108 ºC; IR (cm^{-1}, KBr pellet): 3418(m), 3248(w), 3063(w), 3016(w), 2885(m), 2824(m), 1628(vs), 1574(w), 1489(w), 1443(m), 1373(m), 1265(vs), 1180(w), 1080(m), 1041(m), 910(m),756(vs) (Figure A-10); ^{1}H NMR (400 MHz, DMSO-d_6) δ ppm: 7.81 (4H, m, ArH), 7.49 – 7.32 (6H, br, ArH), 3.81 (4H, s, 2×CH_2), 2.25 (6H, s, 2×CH_3) (Figure A-11); ^{13}C NMR (100 MHz, DMSO-d_6) δ ppm: 165.22, 141.04, 129.86, 128.56, 126.90, 53.26, 15.78 (Figure A-12).

3A.2.6 Synthesis of (1*E*,1'*E*)-*N*,*N*'-(butane-1,4-diyl)bis(1-phenylmethanimine) (L3a)[20]

1,4-Diaminobutane (1.0 mL, 10 mmol) was added dropwise to a solution of benzaldehyde (2.0 mL, 20 mmol) in ethanol (40 mL). The mixture was refluxed for 6 hours. The solvent was

removed under vacuum and the brown color semi-solid product was recrystallized from hexane. Yield: 49%; Melting point: 50-51 ºC; IR (cm^{-1}, KBr pellet): 3394(w), 3271(w), 3055(w), 3024(w), 2932(m), 2847(m), 2646(w), 1643(vs), 1605(w), 1574(w), 1443(s), 1381(w), 1288(w), 965(w), 756(vs) (Figure A-13); ^{1}H NMR (400 MHz, DMSO-d_6) δ ppm: 8.34 (2H, d, J = 1.4 Hz, imine CH), 7.83 – 7.65 (4H, m, ArH), 7.44 (6H, br, ArH), 3.60 (4H, td, J = 5.2, 2.6 Hz, 2×CH_2), 1.96 – 1.47 (4H, m, 2×CH_2) (Figure A-14). ^{13}C NMR (100 MHz, DMSO-d_6) δ ppm: 161.07, 136.61, 130.97, 129.10, 128.27, 60.82, 28.80 (Figure A-15).

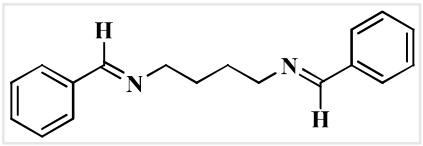

3A.2.7 Synthesis of (1*E*,1'*E*)-*N*,*N*'-(butane-1,4-diyl)bis(1-phenylethan-1-imine) (L3b)

1,4-Diaminobutane (1.0 mL, 10 mmol) was added dropwise to a solution of acetophenone (2.3 mL, 20 mmol) in ethanol (40 mL). The mixture was refluxed for 6 hours. The solvent was removed under vacuum and the green color semi-solid product was recrystallized from hexane. Yield: 50%; Melting point: 61-62 ºC; IR (cm^{-1}, KBr pellet): 3418(m), 3240(w), 3086(w), 3047(w), 2932(m), 2878(m), 1628(vs), 1574(w), 1489(w), 1443(w), 1350(m), 1281(m), 1180(w), 1080(w), 918(w), 764(vs) (Figure A-16); ^{1}H NMR (400 MHz, DMSO-d_6) δ ppm: 7.89 – 7.74 (4H, m, ArH), 7.47 – 7.29 (6H, m, ArH), 3.48 (4H, t, J = 5.7 Hz, 2×CH_2), 2.20 (6H, s, 2×CH_3), 1.80 (4H p, J = 3.5 Hz, 2×CH_2) (Figure A-17). ^{13}C NMR (100 MHz, DMSO-d_6) δ ppm: 164.23, 141.14, 129.74, 128.52, 126.86, 51.73, 29.24, 15.44 (Figure A-18).

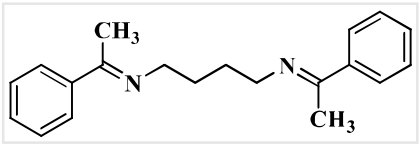

3A.2.8 Synthesis of (1*E*,1'*E*)-*N*,*N*'-(hexane-1,6-diyl)bis(1-phenylmethanimine) (L4a)[20]

Hexamethylene diamine (1.4 mL, 10 mmol) was added dropwise to a solution of benzaldehyde (2.0 mL, 20 mmol) in ethanol (40 mL). The mixture was refluxed for 6 hours. The solvent was removed under vacuum and the brown semi-solid product was recrystallized from hexane. Yield: 48%; Melting point:170-171 ºC; IR (cm^{-1}, KBr pellet): 3394(w), 3148(m), 3001(w), 2939(w), 2854(w), 2716(w), 2106(w), 1643(s), 1589(w), 1551(vs), 1379(vs), 1234(w), 1173(w), 1065(w), 949(w), 825(s) (Figure A-19); ^{1}H NMR (400 MHz, DMSO-d_6) δ ppm: 7.98 – 7.81 (m, 4H), 7.33 (dd, J = 9.9, 6.6 Hz, 1H), 2.77 (t, J = 7.4 Hz, 1H), 1.56 (q, J = 7.0 Hz, 1H), 1.38 – 1.19 (m, 1H). 7.89 (s, 1H), 7.44–7.23 (m, 3H), 2.70 (dd, J = 59.6 Hz, 2H), 1.63-1.45 (m, 2H), 1.40-1.18 (m, 2H) (Figure A-20). ^{13}C-NMR (100 MHz, DMSO) δ ppm: 170.46, 139.62, 129.80, 129.42, 127.83, 27.84, 25.92 (Figure A-21).

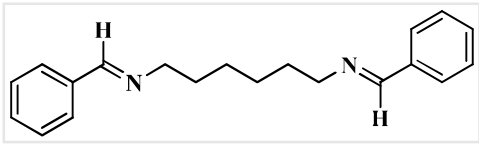

3A.2.9 Synthesis of (1*E*,1'*E*)-*N*,*N*'-(hexane-1,6-diyl)bis(1-phenylethan-1-imine) (L4b)[21]

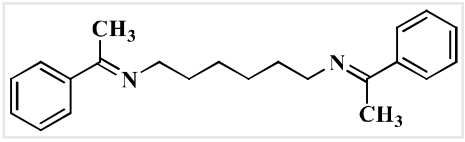

Hexamethylene diamine (1.4 mL, 10 mmol) was added dropwise to a solution of acetophenone (2.3 mL, 20 mmol) in ethanol (40 mL). The mixture was refluxed for 6 hours. The solvent was removed under vacuum and the brown semi-solid product was recrystallized from hexane. Yield: 47%; Melting point: 47-48 ºC. IR (cm^{-1}, KBr pellet): 3811(w), 3433(m), 3256(w), 3055(w), 2924(m), 2854(w), 1628(vs), 1582(w), 1443(w), 1412(m), 1381(m), 1281(w), 794(m), 694(s), 571(w) (Figure A-22); ^{1}H-NMR (400 MHz, DMSO-d_6) δ ppm: 7.87 – 7.69 (4H, m, ArH), 7.50 – 7.28 (6H, m, ArH), 3.46 – 3.40 (4H, m, 2×CH_2), 2.18 (6H, s, 2×CH_3), 1.68 (4H, m, 2×CH_2), 1.57 – 1.40 (4H, m, 2×CH_2) (Figure A-23); ^{13}C NMR (100 MHz, DMSO-d_6) δ ppm: 164.17, 141.14, 129.73, 128.51, 126.85, 51.75, 31.16, 27.55, 15.40 (Figure A-24).

3A.3 Results and discussion

To analyze the relation between the photophysical properties of the compounds (Scheme 3A.1) with their geometry and supramolecular arrangement, the crystal structure description of some compounds was studied. The crystal structures of **L1a**[14], **L1b**[15], **L2b**[16] and **L2c**[22] were reported by other groups, while our group reported the crystal structure description of **L1d**, **L2d** and **L3c**[19]. The following features were observed while analyzing the structural aspects of these compounds.

3A.3.1 Crystal structure analysis of L1a[14]

The compound **L1a** has an orthorhombic *Pbcn* space group and only half of the molecule is present in the asymmetric unit (Figure 3A.4a). The molecules in **L1a** are packed in such a way that the N-N bonds of the adjacent molecules are arranged in parallel fashion with a distance of 3.810 Å between the two nitrogen atoms of the neighboring molecules (Figure 3A.4b). The aromatic moieties of the two adjacent molecules have inclined/tilted arrangements with a centroid-to-centroid distance of 4.873 Å (Figure 3A.4c). This results in a 1D arrangement of the molecules, which are further assembled in 3D via aromatic interactions between the inclined aromatic rings (centroid-to-centroid distance of 5.011 Å) (Figure 3A.4c).

3A.3.2 Crystal structure analysis of L1b[15]

The compound **L1b** is crystallized in monoclinic $P2_1/n$ space group with one molecule in the asymmetric unit. The molecule of **L1b** has non-planar geometry, where the C–N–N–C torsion

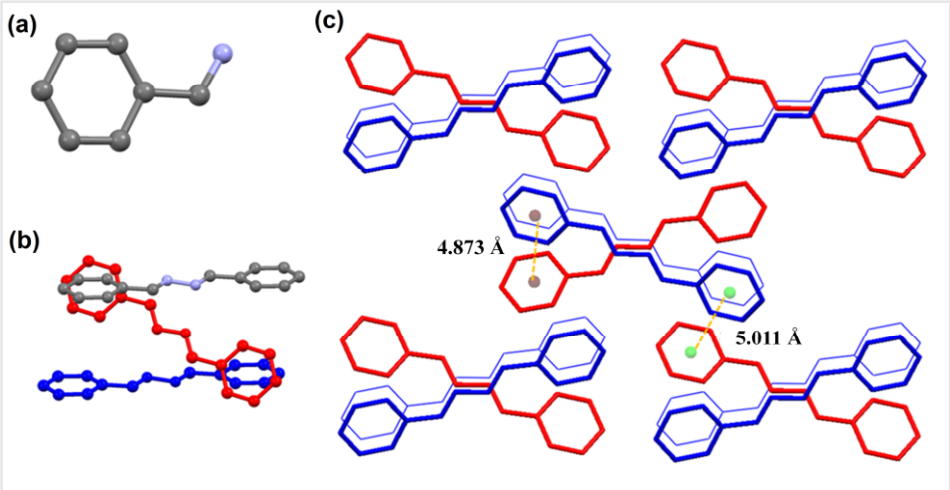

Figure 3A.4: Illustration of crystal structure of **L1a**[14]: (a) Asymmetric unit of **L1a**; (b) Arrangement of adjacent molecules; (c) Packing of the molecules (figures were generated from the data obtained from CCDC No. 1118104)

angle is 138.7° and the two phenyl rings of the molecule are inclined at an angle of 64.6° (Figure 3A.5a). Although inclined face-to-face stacking of the molecules has been observed in this case, due to the non-planar geometry of the molecules, a significant number of close contacts instigated 3D packing of the molecules (Figure 3A.5c). The phenyl ring of one **L1b** molecule is in the vicinity of phenyl rings of three neighboring molecules such that the centroid–to–centroid distances between the aromatic rings are in the range of 4.6-4.9 Å (Figure 3A.5b).

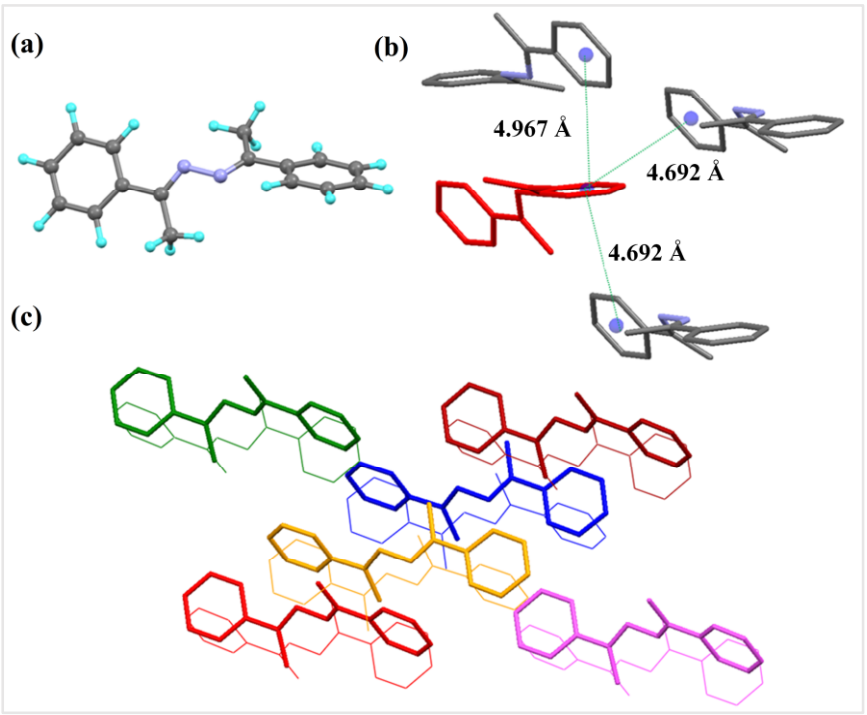

Figure 3A.5: Illustration of crystal structure of **L1b**[15]: (a) Asymmetric unit of **L1b** showing the non-planar geometry of the molecule; (b) Centroid-to-centroid distance between the adjacent aromatic rings; (c) Packing of the molecules (figures were generated from the data obtained from CCDC No. 1207284)

3A.3.3 Crystal structure analysis of L1d[19]

The crystal structure analysis of **L1d** showed that there are three molecules in the asymmetric unit, which are differed in the orientation of pyridyl and imine moieties. The two molecules are arranged parallelly such that they form a dimer (Figure 3A.6). The distances between the C=N bonds of the two molecules are 3.906 Å and 3.943 Å, while the centroid-to-centroid distances between two pyridyl rings are 3.888 Å and 4.009 Å. The third type of molecule interacts with the other two molecules via C–H•••N and aromatic π•••π interactions and helped in the formation of dimers.

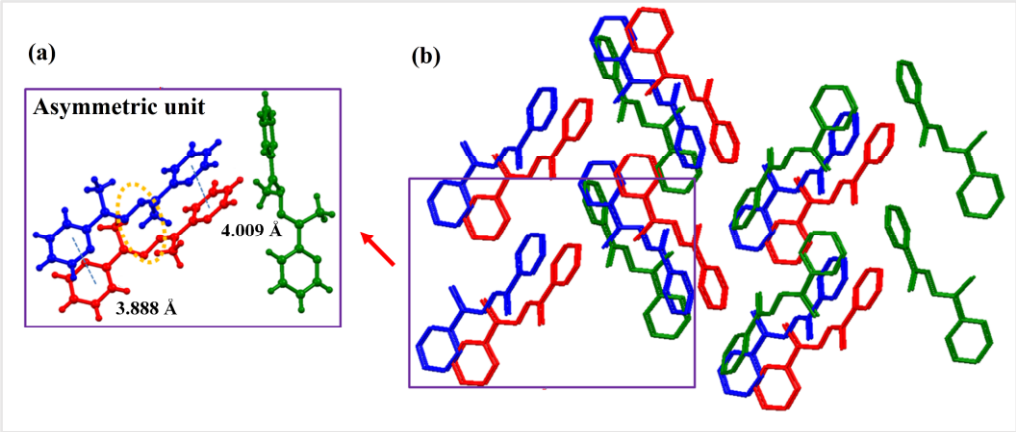

Figure 3A.6: Illustration of crystal structure of **L1d**[12]: (a) Packing of the molecules (hydrogen atoms are removed for clarity); (b) Three types of molecules of **L1d** are present in the asymmetric unit, which is shown in different colors. (figures were generated from the data obtained from CCDC No. 963345)

3A.3.4 Crystal structure analysis of L2b[16]

The compound **L2b** is crystallized in *P2₁/n* space group with half of the molecule in the asymmetric unit (Figure 3A.7a). The ethyl group in the molecule adopted all *anti* conformation. The molecules are stacked in parallel manner to form a one-dimensional network (Figure

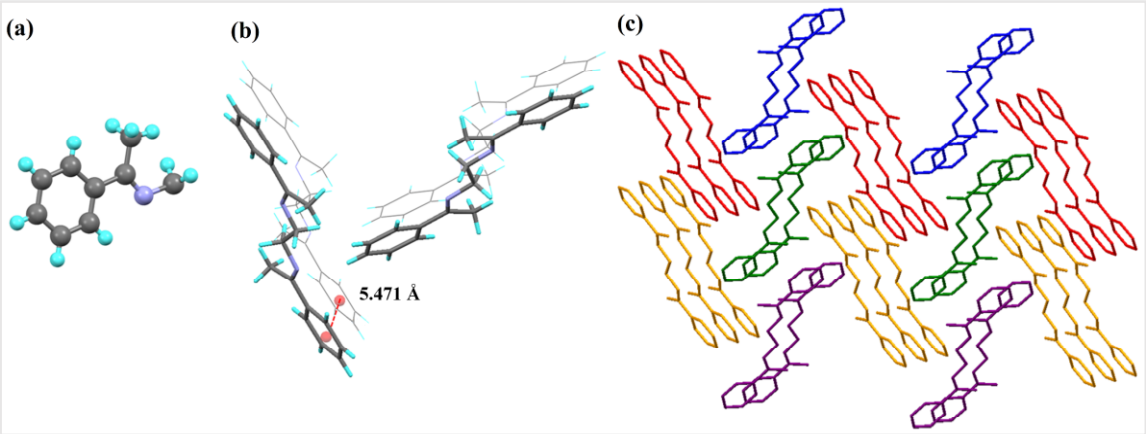

Figure 3A.7: Illustration of crystal structure of **L2b**[16]: (a) Asymmetric unit; (b) 1D arrangement of the molecules: notice that the aromatic centroid-to-centroid distance is more than 5 Å; (c) Herringbone arrangement of **L2b** molecules in crystal packing (figures were generated from the data obtained from CCDC No. 608471)

3A.7b). The 3D packing of the molecules can be viewed as the herringbone arrangement of the one-dimensional networks (Figure 3A.7c).

3A.3.5 Crystal structure analysis of L2d[19]

The crystal structure of **L2d** has been reported by our group[19] and it showed that there are two molecules in the asymmetric unit (Figure 3A.8a). The ethylene spacer of **L2d** adopted *anti* conformation thereby resulting in linear geometry of the molecule. The neighboring molecules are arranged in an offset manner to form a one-dimensional network (Figure 3A.8b). The overall supramolecular network can be viewed as the herringbone arrangement of this one –dimensional network (Figure 3A.8c).

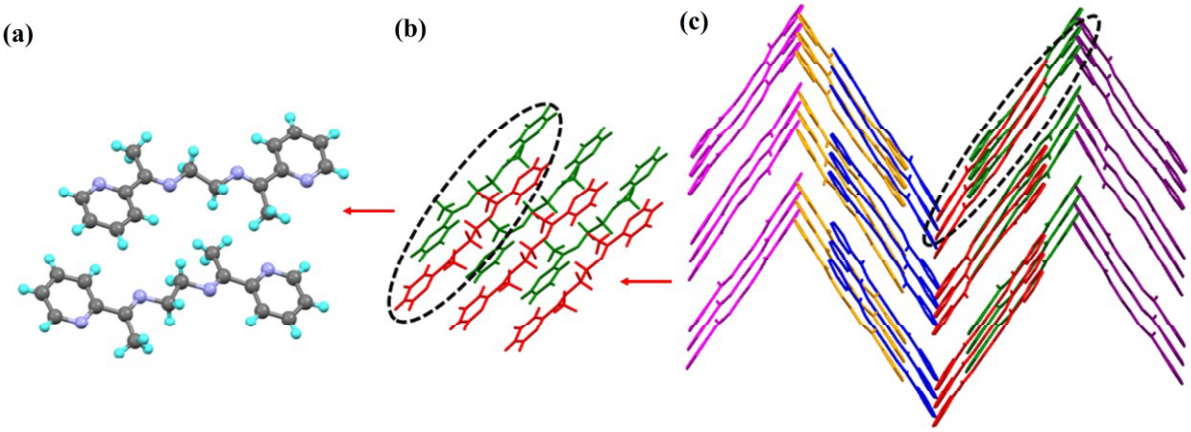

Figure 3A.8: Illustration of crystal structure of **L2d**[12]: (a) Asymmetric unit; (b) Offset arrangement of the molecules to form a 1D network; (c) Herringbone arrangement of the molecules of **L2d** (hydrogen atoms were removed for clarity) (figures were generated from the data obtained from CCDC No. 962823)

3A.3.6 Crystal structure analysis of L2c[22] and L3c[19]

The asymmetric unit in **L2c** has half of the molecule and the ethylene spacer adopts *gauche* conformation. The C–H···N hydrogen bond interactions between the pyridyl N and C–H of methinine triggered the formation of a "non-covalently bonded chromophore" unit (Figure 3A.9a and 3A.9b). The crystal structure analysis of **L3c** showed that it has half of the molecule in the asymmetric unit (Figure 3A.9c). Further, it was observed that the butylene spacer of **L3c** adopted *gauche-anti-gauche* conformation instead of expected all *anti* conformation. The pyridyl–N···HC– (Methinine) interactions produced a non-covalently bonded "macrocyclic" moiety (Figure 3A.9d). The butylene chain conformation allowed the formation of corrugated layers and offset packing of the layers resulted in the overall 3D arrangement of the **L3c** (Figure 3A.9e).

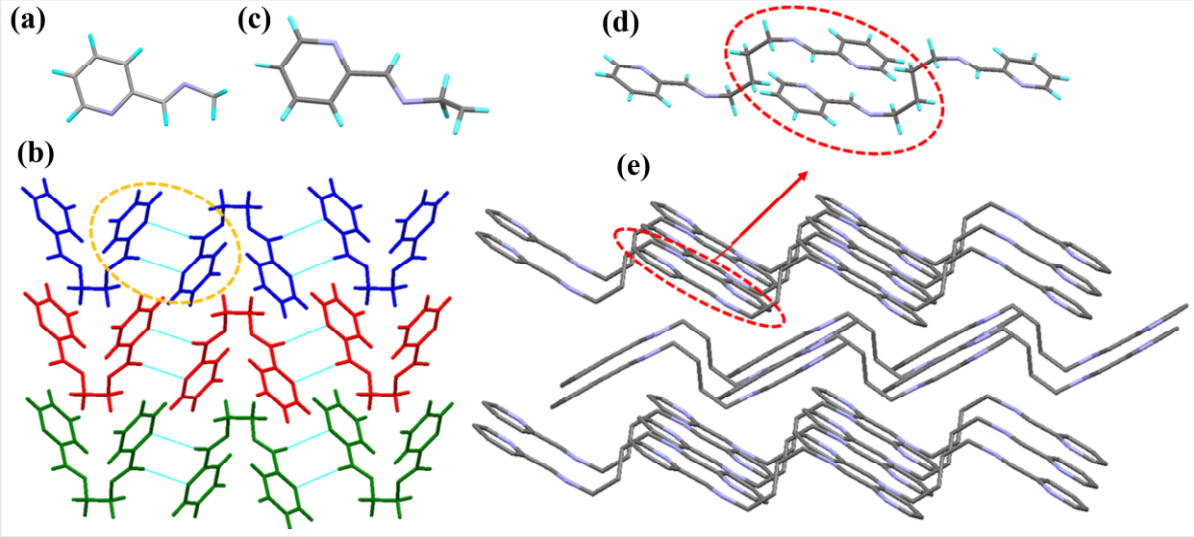

Figure 3A.9: Illustration of crystal structure of **L2c**[19] and **L3c**[12]: (a) Asymmetric unit in **L2c**; (b) Packing of the molecules of **L2c** via C-H···N interactions to form non-covalent macrocyclic moiety; (c) Asymmetric unit in **L3c**; (d) Non-covalent "macrocyclic" moiety in **L3c**; (e) Offset packing of the corrugated layers in **L3c** (hydrogen atoms are removed for clarity) (figures were generated from the data obtained from CCDC No. 721559 (**L2c**) and 930055(**L3c)**

3A.3.7 Powder XRD spectra of the compounds

Powder XRD spectra were recorded for **L1a**, **L1b**, **L2a**, **L2b**, **L3a**, **L3b**, **L4a,** and **L4b**. The experimental powder XRD spectra of the compounds **L1a**, **L1b**, and **L2b** were compared with the calculated powder XRD spectra from the single crystal XRD data. Figure 3A.10 shows the phase purity of the compounds **L1a**, **L1b**, and **L2b**. The experimental spectra of other compounds are shown in Figure A-25.

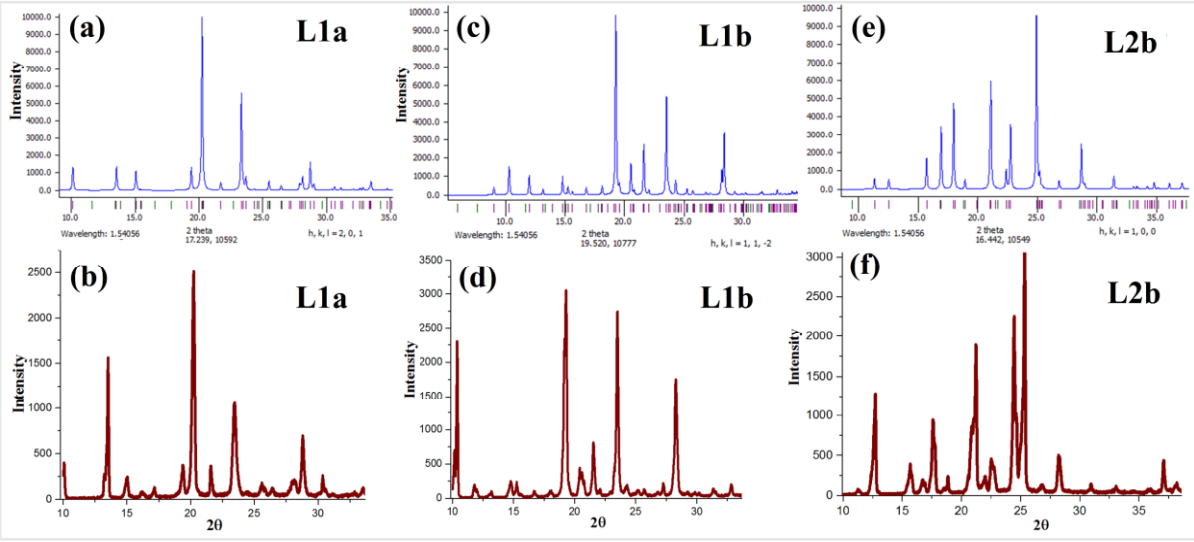

Figure 3A.10: (a) Calculated PXRD of **L1a**; generated from crystal data CCDC No. 1118104; (b) Experimental PXRD of **L1a**; (c) Calculated PXRD of **L1b**; generated from crystal data CCDC No. 1207284; (d) Experimental PXRD of **L1b**; (e) Calculated PXRD of **L2b**; generated from crystal data CCDC No. 608471; (f) Experimental PXRD of **L2b**

3A.3.8 UV-Visible absorption spectra

The solid-state UV-visible spectra of **L1a** showed absorption maxima at 196 nm ($\pi \rightarrow \pi^*$) and 300 nm ($n \rightarrow \pi^*$), while that of **L1b** showed λ_{max} at 206 nm ($\pi \rightarrow \pi^*$) and 266 nm ($n \rightarrow \pi^*$) (Figure 3A.11a, b). The absorption maxima for **L1d** are at 253 nm ($\pi \rightarrow \pi^*$) and 286 nm ($n \rightarrow \pi^*$); which indicates the effect of replacing phenyl group with pyridyl group.[19] The solid-state UV-visible absorption maxima for **L2a**, **L2b**, **L3a**, **L3b**, **L4a,** and **L4b** were in the range 192–194 nm ($\pi \rightarrow \pi^*$) and 223-237 nm ($n \rightarrow \pi^*$) (Table 3A.1, Figure 3A.11c–h), whereas for the **L2** and **L3** compounds with pyridyl group, the λ_{max} was observed in the range of 232–235 nm ($\pi \rightarrow \pi^*$) and 269–271 nm ($n \rightarrow \pi^*$).[19]

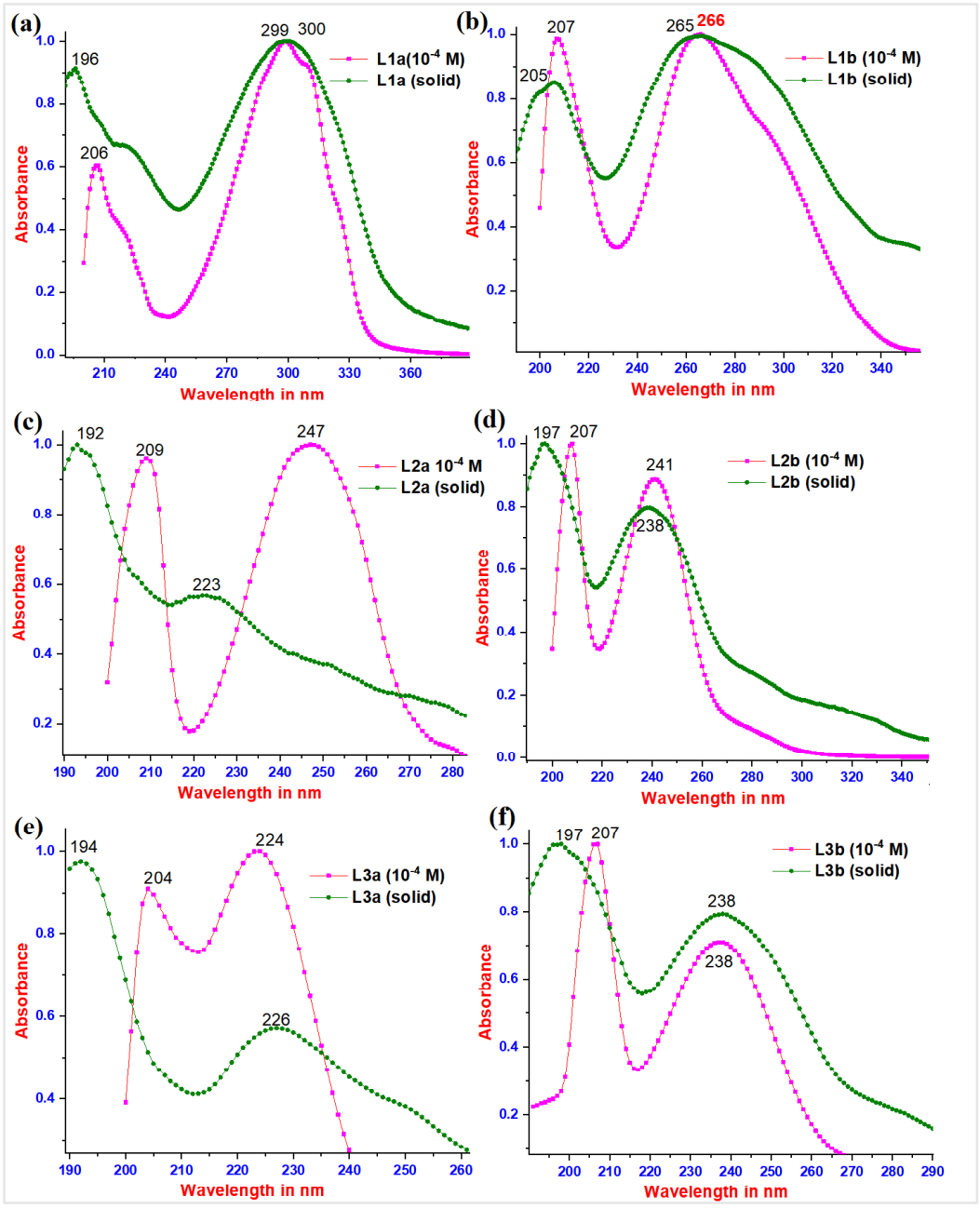

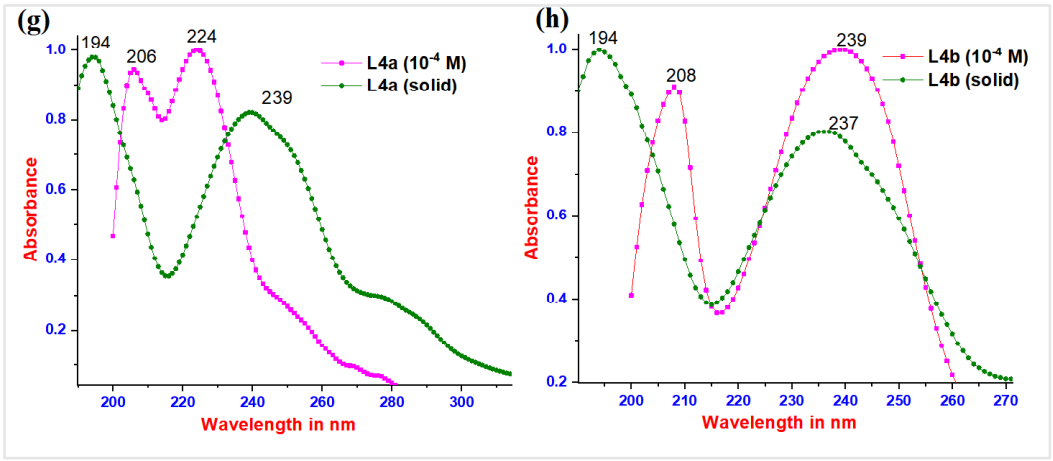

Figure 3A.11: UV-Visible absorption spectra of (a) **L1a,** (b) **L1b**, (c) **L2a**, (d) **L2b**, (e) **L3a**, (f) **L3b,** (g) **L4a**, (h) **L4b** in solid-state and in 1×10^{-4} M solution

The UV-visible absorption spectra in a methanolic solution for the compounds **L1a**, **L1b**, **L2a**, **L2b**, **L3a**, **L3b**, **L4a,** and **L4b** showed red shift (7–12 nm) in the $\pi \rightarrow \pi^*$ peak position compared to their solid-state spectra (Figure 3A.11); which indicates the possibility of parallel stacking of aromatic rings in solid-state to form face-to-face stacking of the aromatic moieties/H-aggregates.[23]

Table 3A.1: UV-Visible absorption maxima for compounds **L1a**, **L1b**, **L2a**, **L2b**, **L3a**, **L3b**, **L4a** and **L4b**

Compd.	Solid State (λ_{max} in nm)	Compds. in MeOH (10^{-4} M) (λ_{max} in nm)
L1a	196, 300	206, 299
L1b	205, 265	207, 266
L2a	192, 223	209, 247
L2b	197, 238	207, 241
L3a	194, 226	204, 224
L3b	197, 238	207, 238
L4a	194, 239	206, 224
L4b	194, 236	208, 239

3A.3.9 Photoluminescence spectra of L2a and L2b

The PL spectra of **L2a** and **L2b** in solid state as well as in methanolic solutions showed the enhanced emission with an increase in concentration. The observation from the concentration dependent PL spectra of **L2a** showed the appearance of a new peak on increasing concentration. For 1×10^{-4} M solution, at excitation wavelength 300 nm, structured bands with λ_{max} 330 nm and 364 nm were observed in PL spectra, whereas at 1×10^{-3} M concentration, an extra shoulder peak appeared at 426 nm. In case of 5×10^{-2} M solution, band at around 359 nm disappeared completely and the only peak at 426 nm was observed (Table 3A.2). But when the excitation wavelength was fixed at 450 nm, concentration lower than 1×10^{-3} M did not show any emission, and on increasing the concentration to 1×10^{-1} M, an intense emission peak appeared at 518 nm (Figure 3A.12a and 3A.12b). The PL spectra of **L2b** showed a

structured emission spectrum (λ_{max} at 330 and 365 nm) at a concentration of 1×10^{-4} M, when the excitation wavelength is 300 nm, while a shoulder peak at 424 nm was appeared for 1×10^{-3} M solution. On changing the excitation wavelength to 450 nm, 1×10^{-1} M solution showed an intense peak at 500 nm (Figure 3A.12c and 3A.12d). The PL spectra of **L2c** and **L2d** were reported previously by our group. The PL spectra of **L2d** showed an increase in emission intensity along with a red shift of the peaks and the solid-state PL spectra showed a λ_{max} at 453 nm when the excitation wavelength is 400 nm. In the PL spectra of **L2c,** a new peak appeared on increasing concentration. It was suggested that the presence of pyridyl group resulted in C–H/N interaction and hence a non-covalently bonded species appeared at high concentration.[19]

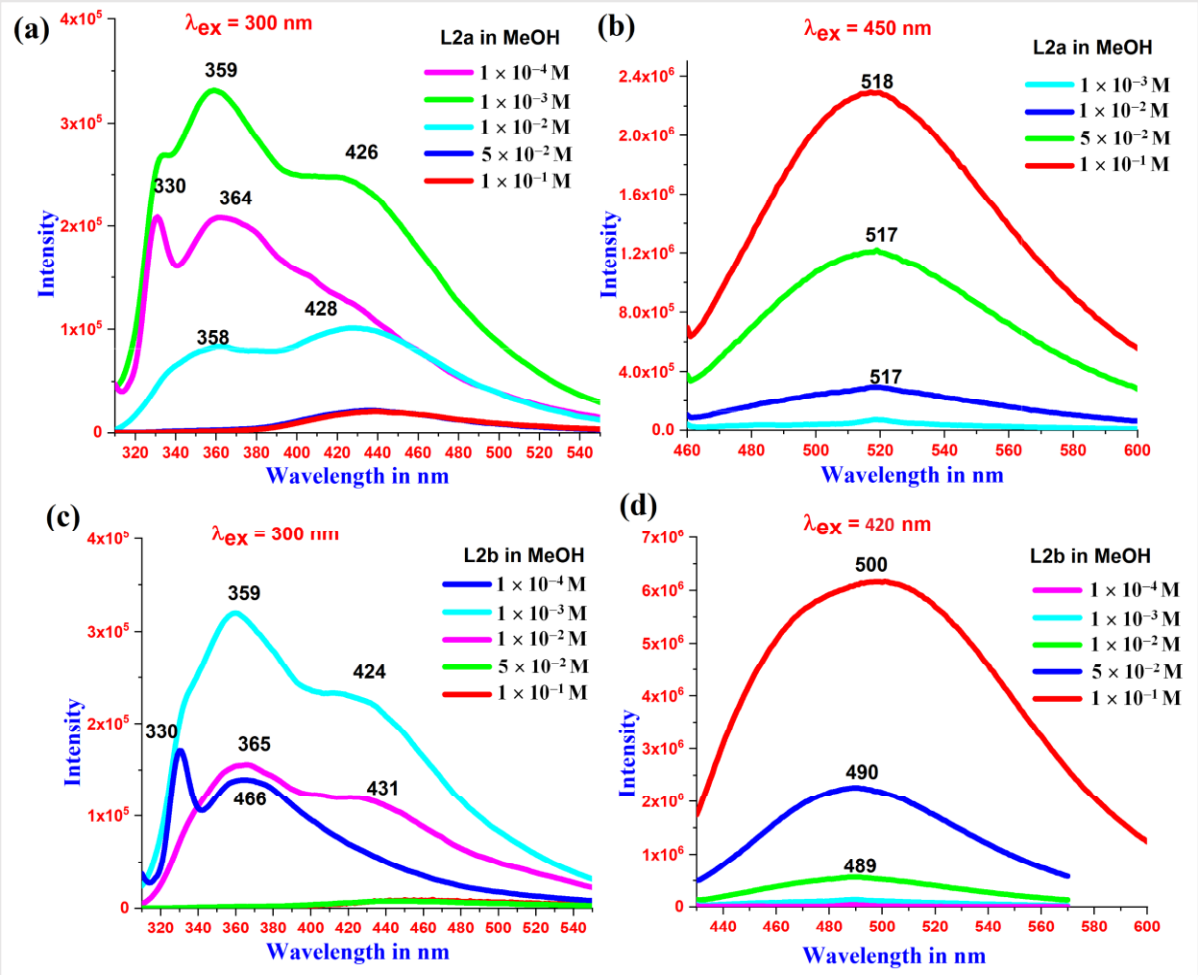

Figure 3A.12: PL spectra of **L2a** (a) λ_{ex} = 300 nm, (b) λ_{ex} = 450 nm and **L2b** (c) λ_{ex} = 300 nm , (d) λ_{ex} = 420 nm at different concentrations

3A.3.10 Photoluminescence spectra of L3a, L3b, L4a, and L4b

The PL spectra of **L3a**, **L3b**, **L4a,** and **L4b** in methanolic solution also showed enhanced-emission on increasing the concentration. The compound **L3a** showed a strong emission

spectrum at λ_{max} 514 nm (excitation wavelength at 440 nm) with a 1×10^{-1} M concentration, while **L3b** showed the emission maxima at 508 nm (excitation wavelength at 450 nm) with a 1×10^{-1} M concentration (Figure 3A.13; Table 3A.2). The compounds **L4a** and **L4b** at a concentration of 1×10^{-1} M also showed emission maxima at 519 nm (excitation wavelength at 450 nm) and 420 nm (excitation wavelength at 493 nm), respectively (Figure 3A.14). The PL spectra of **L3c** showed the appearance of a new peak at high concentration while **L3d** showed intensity increase along with red shift as reported previously by us.

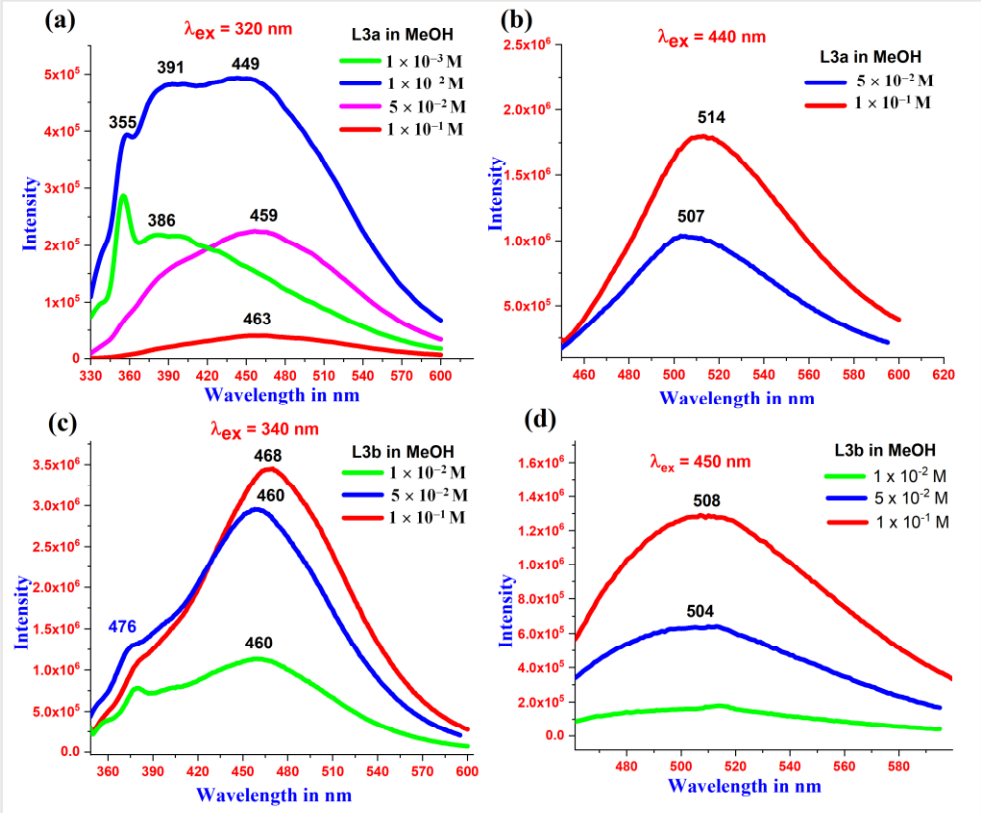

Figure 3A.13: PL spectra of **L3a** (a) λ_{ex} = 320 nm, (b) λ_{ex} = 440 nm and **L3b** (c) λ_{ex} = 300 nm, (d) λ_{ex} = 420 nm at different concentrations

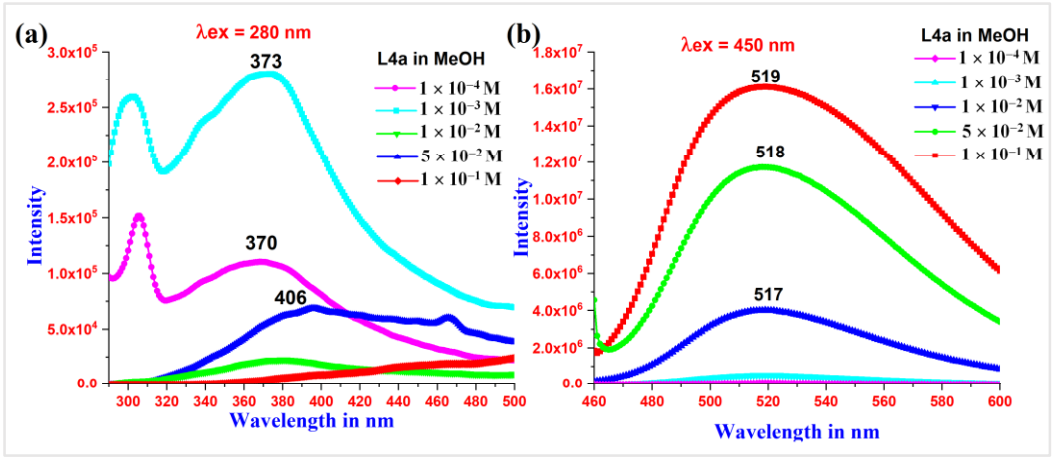

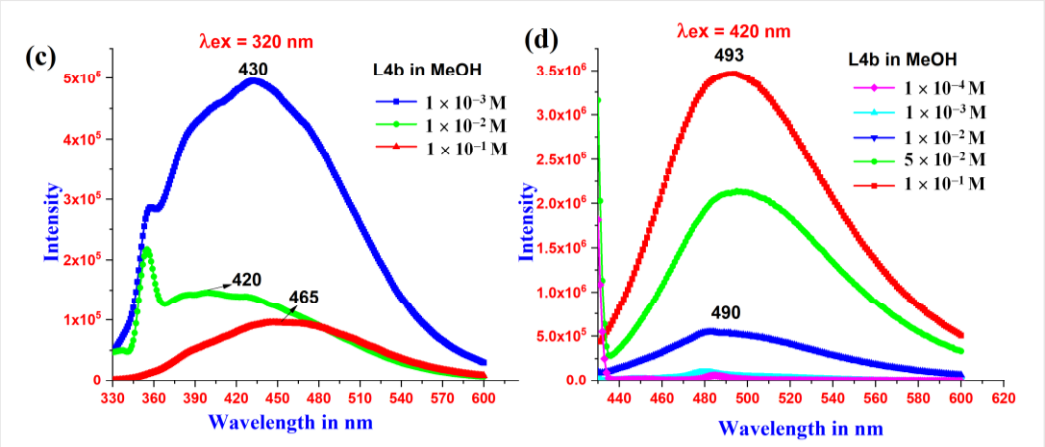

Figure 3A.14: PL spectra of **L4a** (a) λ_{ex} = 280 nm, (b) λ_{ex} = 450 nm and **L4b** (c) λ_{ex} = 320 nm , (d) λ_{ex} = 420 nm at different concentrations

Table 3A.2: λ_{max} in the PL spectra of the compounds (Figure A-26)

Compd.	$\lambda_{max.}$ in Methanolic solution of different concentration (Excitation wavelength; Concentration)		$\lambda_{max.}$ in Solid
L2a	**330**, **364** (300 nm; 10^{-4} M) **518** (450 nm; 10^{-4} M)	**439** (300 nm; 10^{-1} M) **518** (450 nm; 10^{-1} M)	**531** (Excitation: 350 nm)
L2b	**330, 366** (300 nm;10^{-4} M **489** (450 nm;10^{-4} M)	**464** (300nm; 10^{-1} M) **500** (450 nm; 10^{-1} M)	**549** (Excitation: 350 nm)
L3a	**365, 386** (320 nm; 10^{-3} M) **479** (420 nm;10^{-4} M)	**463** (320 nm;10^{-1} M) **509** (420 nm; 10^{-1} M)	**524** (Excitation: 440 nm)
L3b	**376, 460** (340 nm; 10^{-2}M) **478** (420 nm; 10^{-4}M)	**382** (320 nm;10^{-1} M) **504** (450 nm; 10^{-2} M)	**510** (Excitation: 450 nm)
L4a	**300, 370** (280 nm; 10^{-4} M) **517** (450 nm; 10^{-4} M)	**514** (280 nm;10^{-1} M) **517** (450 nm; 10^{-2} M)	**515** (Excitation: 440 nm)
L4b	**350, 420** (320 nm; 10^{-3} M) **484** (420 nm; 10^{-4} M)	**465** (320 nm; 10^{-1} M) **490** (420 nm; 10^{-2} M)	**534** (Excitation: 460 nm)

3A.3.11 Solid-state PL spectra

The PL spectra of compounds **L1a**, **L1b**, **L2a**, **L2b**, **L3a**, **L3b**, **L4a,** and **L4b** were recorded in their powder form and crystalline form to get a comparative analysis of the emissions in different states. Compounds **L1a** and **L1b** did not show any PL spectra in powder as well as in the crystalline state. The solid-state PL spectra of **L2a** showed an intense peak at 531 nm when the excitation wavelength was fixed at 350 nm, while **L2b** showed an intense peak at 549 nm. The solid-state PL spectra of **L2a**, **L2b**, **L3a**, **L3b**, **L4a,** and **L4b** are shown in Figure 3A.15. Table 3A.2 and Table A-1 show the comparison of λ_{max} for the compounds in solid-state and

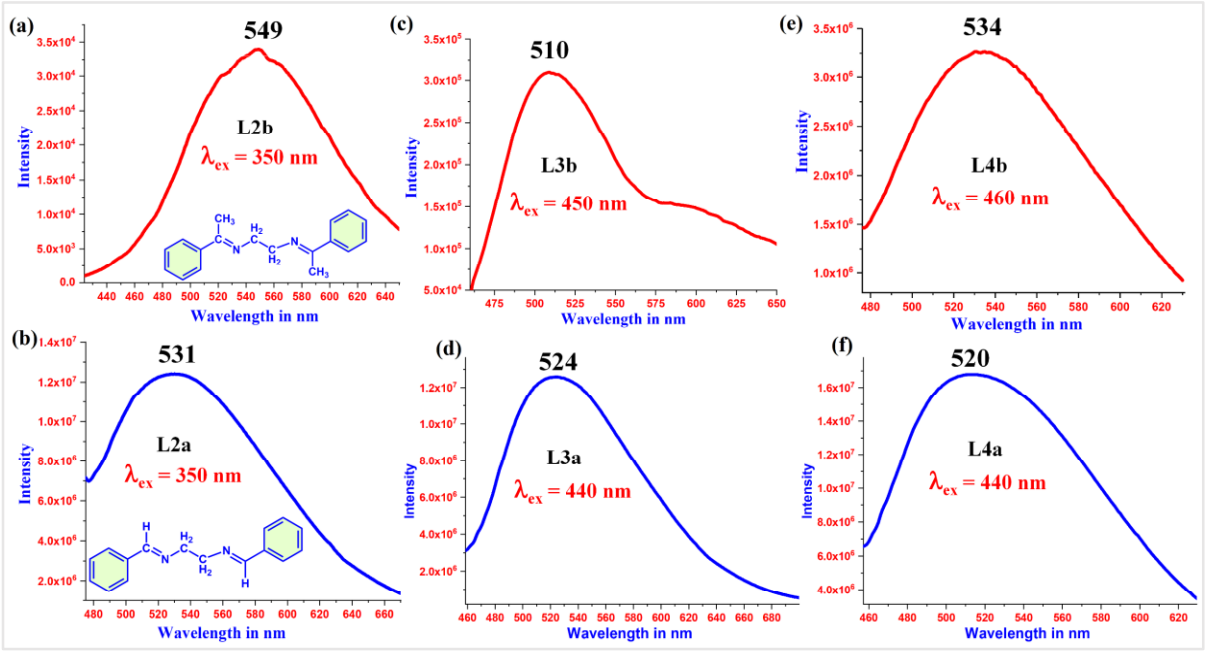

Figure 3A.15: Solid-state PL spectra of (a) **L2b**, (b) **L2a**, (c) **L3b**, (d) **L3a**, (e) **L4b** and (f) **L4a**

3A.3.12 Concentration and excitation energy dependence of PL

The steady-state PL measurements have shown that the emission of the compounds depends on concentration as well as excitation wavelength. On increasing the concentration, at an excitation wavelength around 300 nm, a red shift of emission maxima is observed along with the disappearance of the peak in the region of 300 nm (Table 3A.2). Figure 3A.16 shows the normalized absorption and emission spectra of compound **L2a** and **L2b**. The absorption and emission wavelengths have very little overlap in the 300 nm range.

Table 3A.3 shows the molar extinction coefficients of UV-visible spectra of **L2a** for wavelengths near 300 nm. Although the molar extinction coefficient values are very less in the 300 nm region, reabsorption can be expected at higher concentrations and to some extent this may be the reason for the disappearance of peak at high concentration. Figure A-27 and Table A-2 show the overlap of absorption and emission spectra (at an excitation energy ~300 nm) and molar extinction of UV-vis spectra in the wavelength region around 300 nm, respectively for the compounds **L3a**, **L3b**, **L4a,** and **L4b**. Further, the dependence of emission

Table 3A.3: Molar extinction coefficient of UV-visible spectra of **L2a** in wavelengths near 300 nm

Compd.		Molar extinction coefficient ($\in$)($M^{-1}cm^{-1}$)	Wavelength in nm
L2a	10^{-3} M	**195.2**	**330**
	10^{-4} M	**829** **1095** 3533 4793	**330** **300** 289 280
	10^{-5} M	**3190** **4510** 7970 10610	**330** **300** 289 280

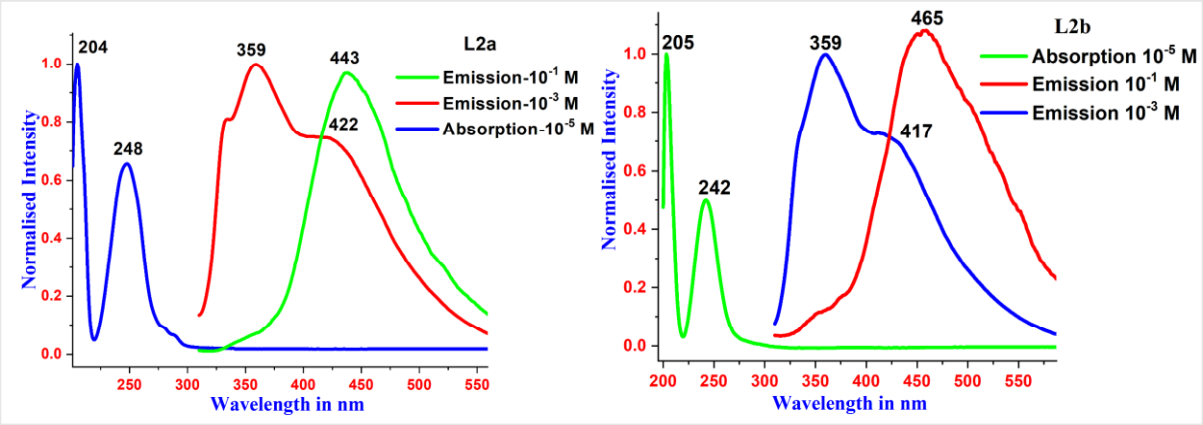

Figure 3A.16: Normalized absorption and emission spectra (at excitation λ = 300 nm) of (a) **L2a** and (b) **L2b**

wavelength on the excitation wavelength is observed from Tables 3A.2 and A-1. The dependence is more pronounced at lower concentrations. In PL spectra of **L2a**, at 1×10^{-4} M concentration, emission maxima are observed at 330 nm and 364 nm (when the excitation wavelength is 300 nm) while emission maxima are observed at 518 nm (when the excitation wavelength is 450 nm). This dependence clearly shows the formation of aggregate species, which are responsible for different emission peaks at different excitation energies.

3A.3.13 Time-resolved fluorescence technique for lifetime analysis

With the help of the time-correlated single-photon counting (TCSPC) technique, we have measured the excited-state decay curve of the compounds (Figure A-28 to A-33). The compounds showed a tri-exponential decay with three lifetimes in the range of 1.0–2.0 ns, 4.0–7.0 ns and 0.1–0.2 ns at concentrations more than 1×10^{-4} M. The shortest lifetime may be attributed to the deactivation (quenching) of excited aromatic groups while the longer lifetime is associated with the unquenched decay of the compounds. Tables 3A.4 and A-3 summarize the lifetime measurements of the compounds. Methanolic solution of **L2b** of concentrations 1×10^{-1} M, and 1×10^{-4} M showed a tri exponential decay when excited at 375 nm and emission was monitored at 457 nm, while a bi-exponential decay was observed at a concentration 1×10^{-6} M. The average lifetimes of 1×10^{-1} M, 1×10^{-4} M and 1×10^{-6} M **L2b** solutions are 1.21 ns, 1.17 ns and 0.90 ns respectively (Figure 3A.17). The concentration

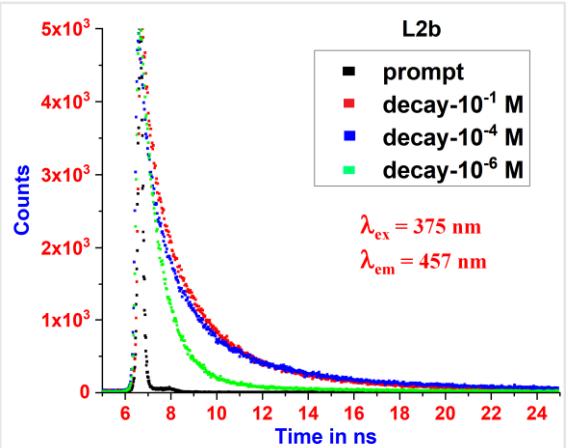

Figure 3A.17: TCSPC decay profiles of **L2b** in different concentration in MeOH with excitation at 375 nm

Table 3A.4: Fluorescence lifetime data for **L2a**, **L2b**, **L3a**, **L3b**, **L4a** and **L4b**

Compound	$\lambda_{Excitation}$ = 375 nm	τ_1 in ns (α_1)	τ_2 in ns (α_2)	τ_3 in ns (α_3)	τ_{avg} in ns (χ^2)
L2a	10^{-1} $\lambda_{Emission}$ 520 nm	**1.55** (0.30)	**5.66** (0.10)	**0.23** (0.60)	**1.15** (1.24)
	10^{-4} $\lambda_{Emission}$ 449 nm	**1.23** (0.35)	**0.26** (0.54)	**4.69** (0.11)	**1.08** (1.05)
L2b	10^{-1} $\lambda_{Emission}$ 457 nm	**1.48** (0.38)	**4.17** (0.13)	**0.23** (0.49)	**1.21** (1.15)
	10^{-4} $\lambda_{Emission}$ 457 nm	**1.51** (0.37)	**5.92** (0.08)	**0.21** (0.55)	**1.17** (1.11)
	10^{-6} $\lambda_{Emission}$ 457 nm	**0.79** (0.97)	**4.56** (0.03)	--	**0.90** (1.40)
L3a	10^{-1} $\lambda_{Emission}$ 500 nm	**1.39** (0.21)	**5.43** (α_2 0.11)	**0.17** (0.0.68)	**1.00** (1.23)
	10^{-2} $\lambda_{Emission}$ 463 nm	**0.99** (0.19)	**4.53** (α_2 0.09)	**0.12** (0.72)	**0.68** (1.11)
L3b	10^{-1} $\lambda_{Emission}$ 477 nm	**2.50** (0.19)	**7.43** (0.24)	**0.24** (0.57)	**2.42** (1.14)
	10^{-5} $\lambda_{Emission}$ 473nm	**6.24** (0.93)	**4.83** (0.07)	-	**0.90** (1.34)
L4a	10^{-1} $\lambda_{Emission}$ 464 nm	**1.93** (0.17)	6.90 (0.11)	**0.15** (0.72)	**1.20** (1.20)
	10^{-4} $\lambda_{Emission}$ 460 nm	**0.86** (0.43)	5.29 (0.11)	**0.19** (0.46)	**1.02** (1.21)
L4b	10^{-1} $\lambda_{Emission}$ 540 nm	**1.42** (0.11)	**5.52** (0.37)	**0.19** (0.52)	**2.29** (1.18)
	10^{-2} $\lambda_{Emission}$ 530 nm	**1.56** (0.09)	**6.02** (0.36)	**0.17** (0.36)	**2.39** (1.29)

dependence of the TCSPC profile of the **L2b** suggested the aggregation of molecules at higher concentrations. The increase in the average lifetime with concentration also recommends that with aggregation in concentrated solution, the unquenched decay processes increase, which may be aggregation induced emission.

3A.3.14 Fluorescence quantum yield

Fluorescence quantum yield was determined for the compounds **L2a**, **L2b**, **L3a**, **L3b**, **L4a** and **L4b** in spectroscopic grade methanol using optically matching solutions of quinine sulfate (Φ_f = 0.546 in 0.5 M H_2SO_4 at an excitation wavelength of 345 nm) as standard. In solid-state, the sample was kept in sample holder cup and the absolute quantum yield was measured. It was observed that the quantum yields of the compounds in dilute solution (1×10^{-4} M in MeOH) were in the range of 0.89–1.98, while on increasing the concentration to 1×10^{-1} M, Φ_f values were observed in the range of 1.52–7.58. The absolute quantum yields in solid-state showed a further increase and values were in the range 2.28–18.68. An interesting trend was observed in the quantum yield for these compounds (Table 3A.5). The compounds **L2a**, **L3a,** and **L4a** showed a higher quantum yield than that of **L2b**, **L3b,** and **L4b**, respectively. Further, on increasing the alkylene spacer length, the quantum yield was observed to increase.

Table 3A.5: Absolute quantum yields in solution and solid states

Compd. (λ_{ex}, λ_{em})	10^{-4} M	10^{-1} M	Solid	Compd. (λ_{ex}, λ_{em})	10^{-4} M	10^{-1} M	Solid
L2a (Φ_f)	1.06	4.04	5.81	**L2b** (Φ_f)	0.89	1.52	2.28
Excitation	300 nm	450 nm	350 nm	Excitation	300 nm	450 nm	350 nm
Emission	365 nm	515 nm	530 nm	Emission	365 nm	515 nm	545 nm
L3a (Φ_f)	1.24	5.48	13.57	**L3b** (Φ_f)	1.09	2.68	9.98
Excitation	320 nm	440 nm	440 nm	Excitation	320 nm	450 nm	420 nm
Emission	380 nm	505 nm	524 nm	Emission	390 nm	505 nm	492 nm
L4a (Φ_f)	1.98	7.58	18.68	**L4b** (Φ_f)	1.32	4.48	14.46
Excitation	340 nm	450 nm	450 nm	Excitation	340 nm	420 nm	460 nm
Emission	370 nm	515 nm	515 nm	Emission	370 nm	490 nm	530 nm

3A.3.15 Correlating the enhanced emission of the compounds with their crystal structure

The absence of fluorescence in **L1a**, **L1b**, **L1c,** and **L1d** can be explained by observing their crystal structures. In the solid-state, the **L1a** molecule has planar geometry. The aromatic rings of the neighboring molecules are tilted where inclined face-to-face stacking is observed. The UV-visible absorption maxima of crystalline solid **L1a** showed a blue shift compared to that in MeOH (1×10^{-4} M). Both the crystal structure as well as the absorption spectra of **L1a** indicated the formation of H-aggregates in solid-state as well as in concentrated solution, which may be attributed to the absence of fluorescence. In the case of **L1b**, the non-planar geometry of the molecule along with face-to-face stacking of the molecules has resulted in quenching of fluorescence, while in **L1d**, quenching of fluorescence is explained by the dimer formation in the solid-state (Scheme 3A.2). Although the crystal structure of **L1c** is not reported, we can speculate that non-radiative decay is due to the head-to-head arrangement of the molecules. In the solid-state, molecules of **L2b** attain planarity with face-to-face stacking. This is similar to the formation of H-aggregates, which are defined by the parallel alignment of the molecules and blue-shifted absorption bands.

The blue-shifted UV-visible bands (about 8 nm) and the crystal structure of **L2b** show that they form H-aggregates. The appearance of the new peak in the PL spectra at higher concentration and red shift of that peak indicates the formation of a new emissive species at high concentration. The crystal structure analysis shows that although H-aggregates are formed in **L2b**, the presence of ethylene spacer is preventing the non-radiative decay processes. The crystal structures of **L2c**, **L3a**, **L3b**, **L4**a, and **L4b** are not reported, but a similar trend in UV-visible absorption spectra and PL spectra indicate that the solid-state arrangement of the molecules may involve parallel face-to-face stacking of the molecules (or H-aggregates)

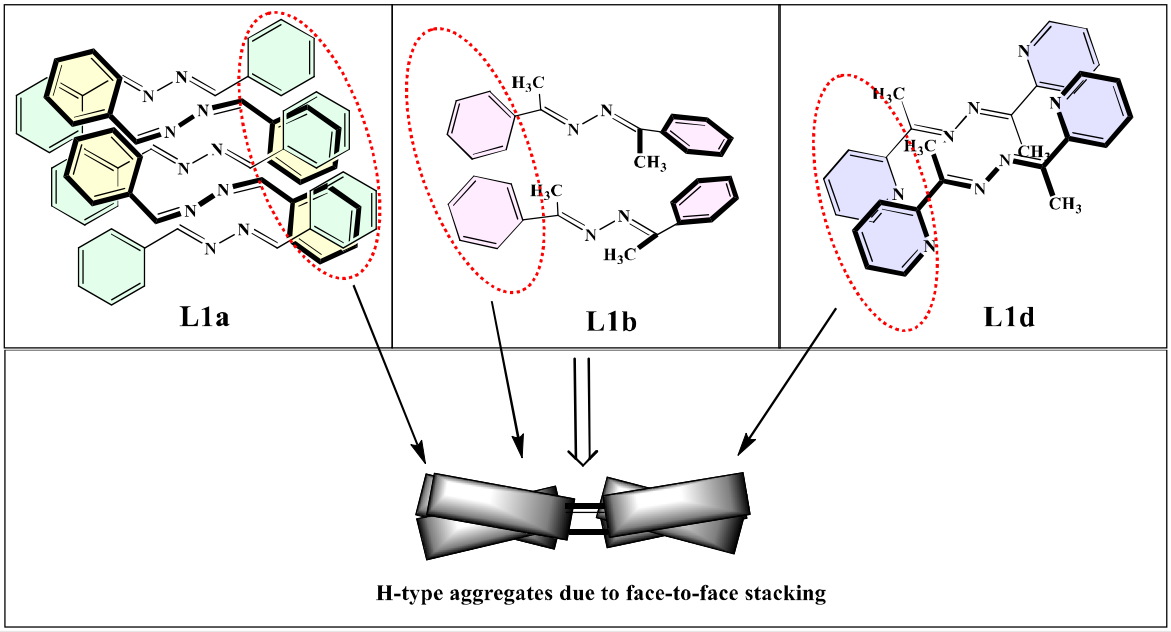

Scheme 3A.2: Arrangement of the molecules of **L1a**, **L1b** and **L1d** in the solid state; notice the face-to-face stacking of the molecules. Although it is inclined in the case of **L1a** and **L1b**, no fluorescence is observed in solid-state

(Scheme 3.A.3). In **L2d,** the attainment of the planar geometry and offset arrangement of molecules resulted in increased emission in PL spectra upon increasing the concentration and in the solid-state, and similar behavior is expected for **L3d** in solid-state (Scheme 3A.4).

In **L2c** and **L3c**, it was reported previously by our group that the formation of a new "chromophore" species in the concentrated solution and in the solid state produced enhancement in the emission intensity. The crystal structure analysis of **L3c** showed that the

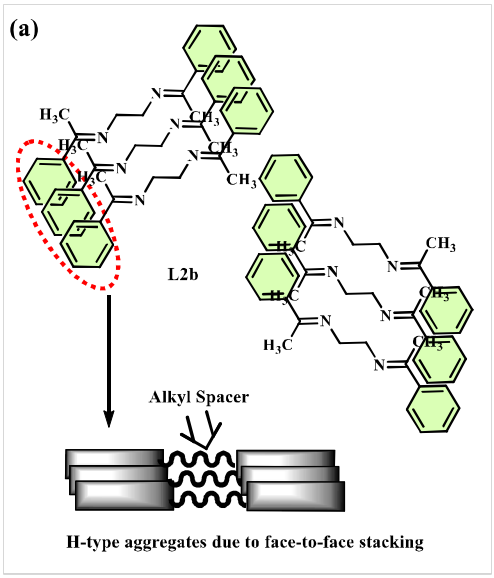

Scheme 3A.3: The face-to-face stacking arrangement of L2b molecules

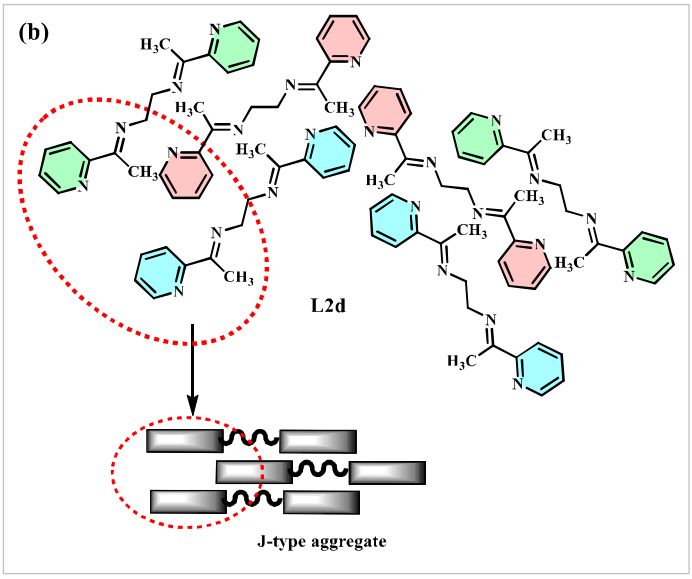

Scheme 3A.4: Arrangement of the molecules of **L2d** and **L3d** in the solid state; Notice the offset stacking of molecules

non-covalent interactions led to the arrangement of the molecules in "non covalently bonded macrocycles" (Scheme 3A.5).

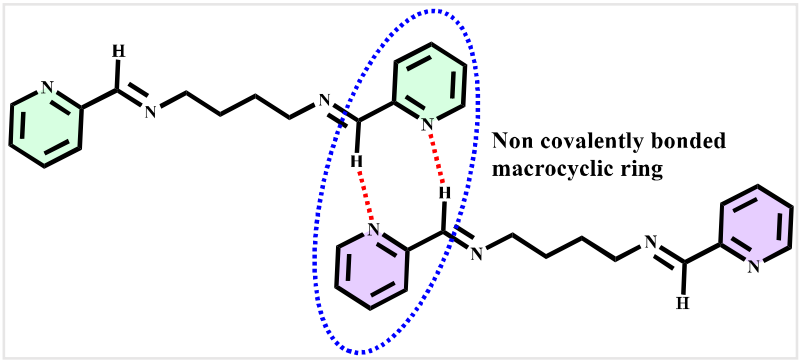

Scheme 3A.5: Arrangement of the molecules of **L2c** and **L3c** in the solid-state; notice the formation of new "chromophore" on aggregation and in the solid-state

3A.3.16 NMR analysis to detect the aggregation in concentrated solution

The effect of changing the concentration on the NMR spectra of aggregating compounds include changes in the chemical shifts, peak shape and intensity of the peaks.[24] The ^{1}H NMR spectra of compounds **L1a**, **L1b**, **L2b,** and **L3b** were recorded at different concentrations in $CDCl_3$. The indication of the possible molecular arrangement on aggregation in concentrated solution may be obtained from the final arrangement of the molecules in the solid-state. The concentration dependent ^{1}H NMR of **L1a** showed that the aromatic protons and the methine protons resonated in deshielded region when the concentration was increased from 0.01 M to 1.0 M (Figure 3A.18)

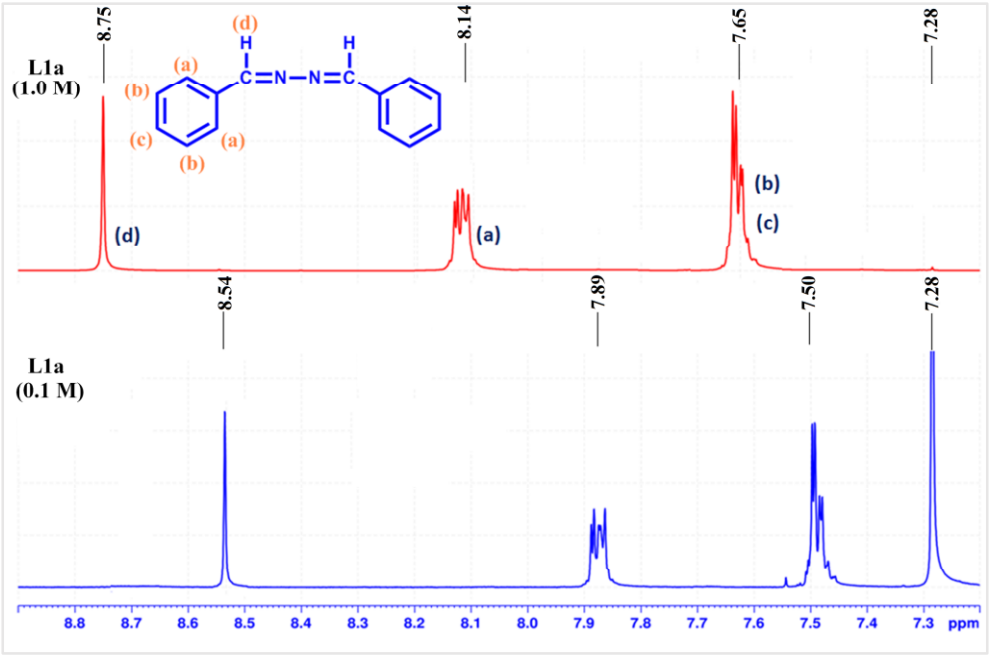

Figure 3A.18: ^{1}H NMR spectra of **L1a** at different concentrations taken in $CDCl_3$

The aggregation of molecules at higher concentrations has affected the chemical shift values of the protons. From the crystal structure analysis of **L1a**, it was observed that the molecules have tilted face-to-face arrangement and the aromatic moieties are clustered together. The concentration dependent ^{1}H NMR spectra of **L2b** and **L3b** was recorded in $CDCl_3$ (Figure 3A.19 and A-52). In both the cases, aromatic protons were shifted towards more deshielded region when the concentration was increased from 0.01 M to 1.0 M, whereas the methyl protons moved in the direction of more shielded region on increasing the concentration. The crystal structure analysis of **L2b** showed parallel stacking of the aromatic rings, which may be associated with the deshielding effects of aromatic protons on increasing concentrations. On observing the structure closely, the herringbone arrangement of the parallel stacked layer resulted in positioning of the methyl groups in such a way that they fall just above the aromatic rings (Scheme 3A.6), which explains the shielding effect of the methyl protons on increasing concentration. The concentration dependent ^{1}H NMR of **L2d** in $CDCl_3$ showed that the increase in concentration from 0.01 M to 1.0 M resulted in the shifting of aromatic protons to the side of shielded region (Figure 3A.20 and A-53). The shielding of aromatic protons in concentrated solutions of **L2d** may be due to the offset arrangement of the molecules. So, face–to–face stacking of aromatic rings is absent in **L2d**, which has brought the deshielding effects in the case of **L1a**, **L2b** and **L3b**.

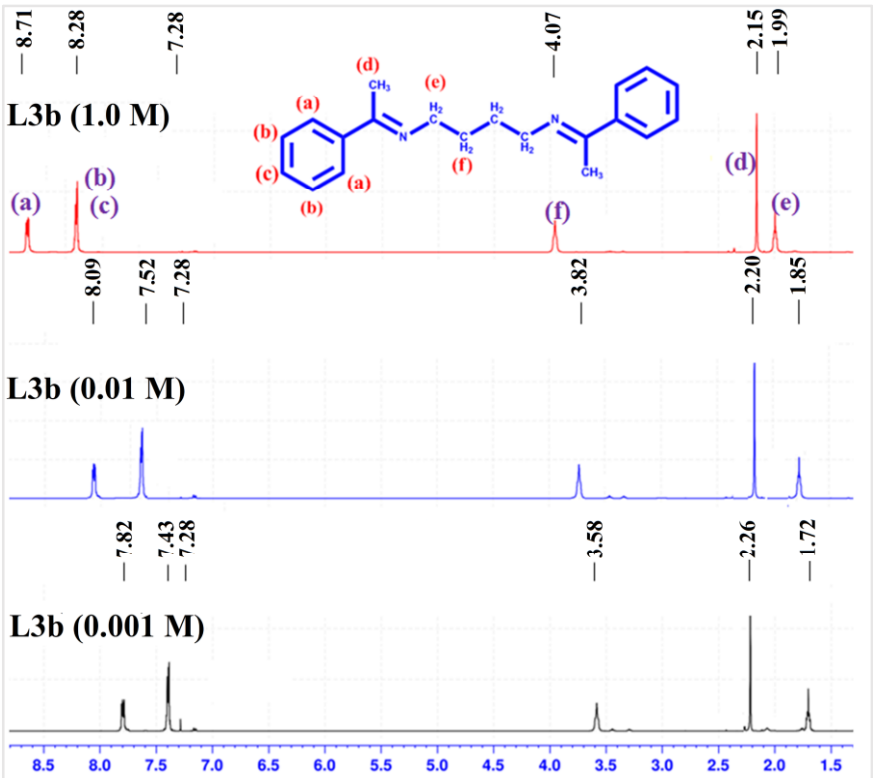

Figure 3A.19: ^{1}H NMR spectra of **L3b** at different concentrations taken in $CDCl_3$

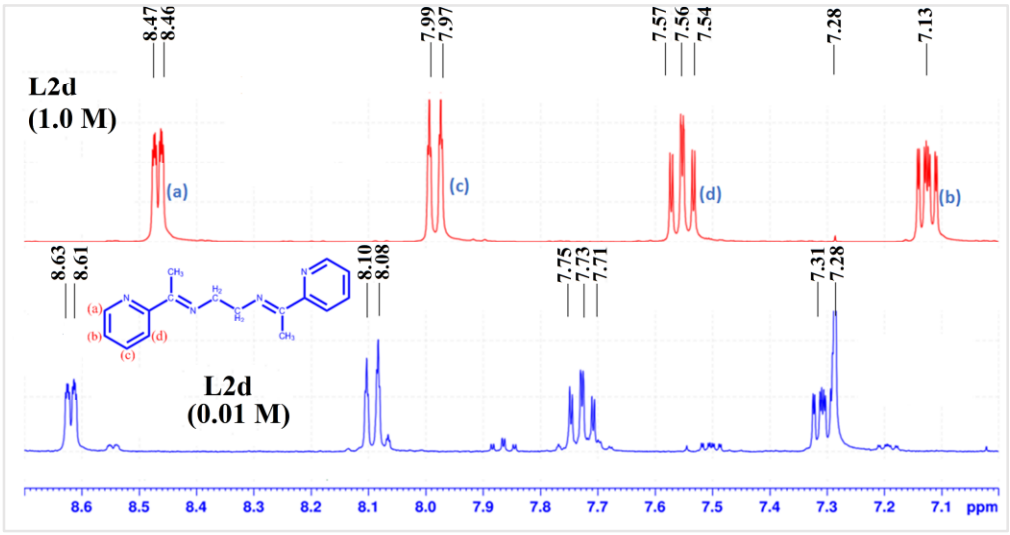

Figure 3A.20: ^{1}H NMR spectra of **L2d** at different concentrations taken in $CDCl_3$

The 2D NOESY spectrum of **L2b** (2.0 M) in $CDCl_3$ was taken to observe the interaction between different types of protons at higher concentrations due to aggregation (Figure 3A.21). The spectrum showed an interaction of the aromatic proton 'a' with 'b' & 'c' and an interaction of aromatic protons ('a', 'b', 'c'), with the methyl protons ('d'). This suggested that at high concentrations, the methyl protons interact with the aromatic protons and a structure similar to Scheme 3A.6 may be possible. Further, the interaction between the aromatic protons also suggests a face-to-face stacking of the molecules at higher concentrations.

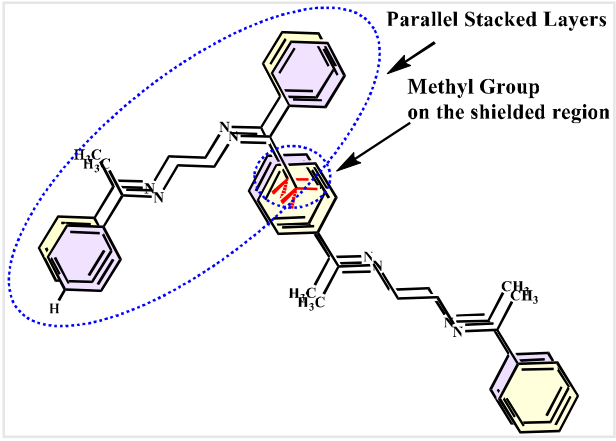

Scheme 3A.6: Arrangement of the molecules in **L2b** and **L3b** resulted in deshielded aromatic proton and shielded methyl protons

3A.4 Conclusions

A systematic study of unique AIE properties of di-Schiff base compounds has been carried out. The crystal structure analysis of some of these compounds has given us the idea about the interplay of non-covalent interactions and crystal packing on the photophysical properties of the compounds. Apart from the compounds with hydrazine spacer i.e., **L1**, all the other compounds have small π-conjugated systems linked with alkylene spacers. In **L1**, where extended conjugation is present throughout the molecule did not show any fluorescence, while other compounds with alkylene spacer showed good emission properties. The emission

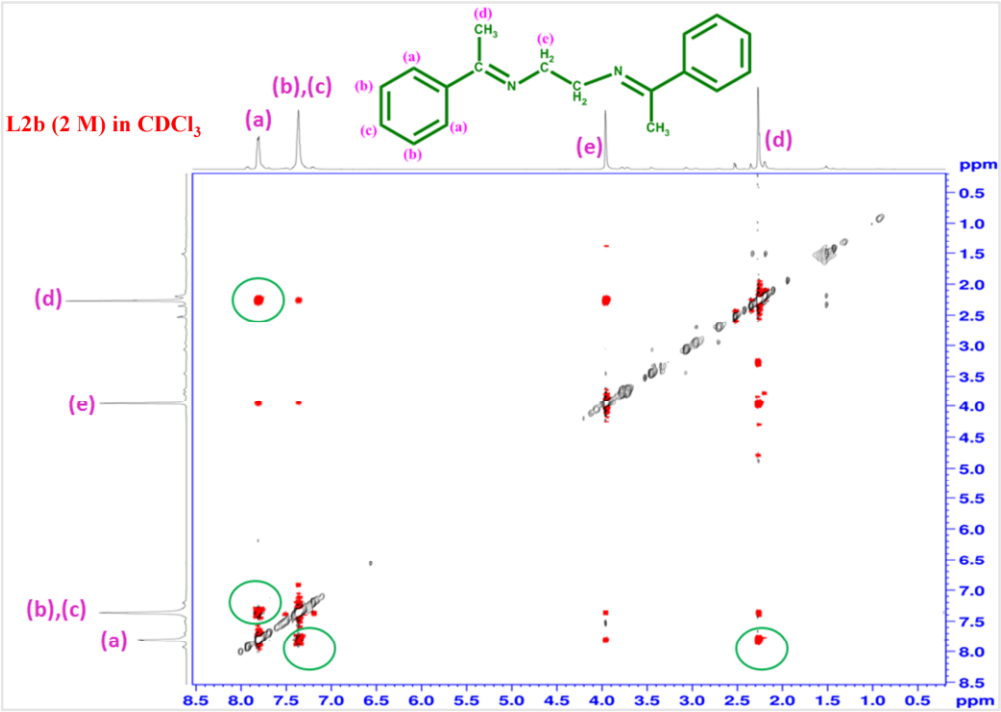

Figure 3A.21: NOESY of **L2b** in $CDCl_3$ at a concentration of 2 M

properties of these compounds are related to the arrangement of the molecules in aggregated states. In **L1**, the H-aggregate formation/dimer formation has resulted in the quenching of fluorescence. In **L2b**, the H-aggregate formation was evident from the crystal structure and UV-visible absorption spectra, but AIE properties were observed. The alkylene spacer in **L2b** is preventing the non-radiative decay processes which is usually observed for H-aggregated systems. The compounds **L2a**, **L3a**, **L3b**, **L4a,** and **L4b** have also been expected to show similar packing as that of **L2b** and the enhanced emission properties of these compounds are attributed to the presence of the alkylene spacers.

3A.5 References

[1] (a) Kelley T., Baude P., Gerlach C., Ender D., Muyres D. H., *Chem. Mater,* **2004**, 16, 4413; (b) Chen C.-T., *Chem. Mater.,* **2004**, 16(23), 4389-4400; (c) Yersin H. *Highly efficient OLEDs with phosphorescent materials*: John Wiley & Sons; **2008**; (d) Kim H. N., Guo Z., Zhu W., Yoon J., Tian H., *Chem. Soc. Rev.,* **2011**, 40(1), 79-93; (e) Wu J., Liu W., Ge J., Zhang H., Wang P., *Chem. Soc. Rev.,* **2011**, 40(7), 3483-3495; (f) Tao Y., Yang C., Qin J., *Chem. Soc. Rev.,* **2011**, 40(5), 2943-2970; (g) Sasabe H., Kido J., *Chem. Mater.,* **2011**, 23(3), 621-630; (h) Schäferling M., *Angew. Chem. Int. Ed.,* **2012**, 51(15), 3532-3554; (i) Zhu M., Yang C., *Chem. Soc. Rev.,* **2013**, 42(12), 4963-4976; (j) Breul A. M., Hager M. D., Schubert U. S., *Chem. Soc. Rev.,* **2013**, 42(12), 5366-5407.

[2] (a) Lam J. L. Z. X. J., *Chem. Commun,* **2001**, 1740; (b) Tang B. Z., Zhan X., Yu G., Sze Lee P. P., Liu Y., Zhu D., *J. Mater. Chem.,* **2001**, 11(12), 2974-2978; (c) Hong Y., Lam J. W. Y., Tang B. Z., *Chem. Soc. Rev.,* **2011**, 40(11), 5361-5388; (d) Hu R., Leung N. L. C., Tang B. Z., *Chem. Soc. Rev.,* **2014**, 43(13), 4494-4562.

[3] (a) An B.-K., Kwon S.-K., Jung S.-D., Park S. Y., *J. Am. Chem. Soc.,* **2002**, 124(48), 14410-14415; (b) Ryu S. Y., Kim S., Seo J., Kim Y.-W., Kwon O.-H., Jang D.-J., Park S. Y., *Chem. Commun.,* **2004**, 2004(1), 70-71; (c) You Y., Huh H. S., Kim K. S., Lee S. W., Kim D., Park S. Y., *Chem. Commun.,* **2008**, 2008(34), 3998-4000; (d) An B.-K., Gihm S. H., Chung J. W., Park C. R., Kwon S.-K., Park S. Y., *J. Am. Chem. Soc.,* **2009**, 131(11), 3950-3957; (e) Chung J. W., An B.-K., Park S. Y., *Chem. Mater.,* **2008**, 20(21), 6750-6755.

[4] (a) Ning Z., Chen Z., Zhang Q., Yan Y., Qian S., Cao Y., Tian H., *Adv. Funct. Mater.,* **2007**, 17(18), 3799-3807; (b) Ning Z., Tian H., *Chem. Commun.,* **2009**, 2009(37), 5483-5495; (c) Wang B., Wang Y., Hua J., Jiang Y., Huang J., Qian S., Tian H., *Chem. Eur. J.,* **2011**, 17(9), 2647-2655.

[5] (a) Du X., Wang Z. Y., *Chem. Commun.,* **2011**, 47(14), 4276-4278; (b) Levitus M., Schmieder K., Ricks H., Shimizu K. D., Bunz U. H. F., Garcia-Garibay M. A., *J. Am. Chem. Soc.,* **2001**, 123(18), 4259-4265.

[6] Kasha M., Rawls H., El-Bayoumi M. A., *Pure Appl. Chem.,* **1965**, 11(3-4), 371-392.

[7] (a) Anthony S. P., Varughese S., Draper S. M., *J. Phys. Org. Chem.,* **2010**, 23(11), 1074-1079; (b) Anthony S., *Chem. Commun,* **2009**, 7500.

[8] Varughese S., *J. Mater. Chem. C,* **2014**, 2(18), 3499-3516.

[9] (a) Hadjoudis E., Mavridis I. M., *Chem. Soc. Rev.,* **2004**, 33(9), 579-588; (b) Cozzi P. G., *Chem. Soc. Rev.,* **2004**, 33(7), 410-421; (c) Andruh M., *Chem. Commun.,* **2011**, 47(11), 3025-3042.

[10] Kawasaki T., Kamata T., Ushijima H., Murata S., Mizukami F., Fujii Y., Usui Y., *Mol. Cryst. Liq. Cryst.,* **1996**, 286(1), 257-262.

[11] (a) Tang W., Xiang Y., Tong A., *J. Org. Chem.,* **2009**, 74(5), 2163-2166; (b) Wei R., Song P., Tong A., *J. Phys. Chem. C,* **2013**, 117(7), 3467-3474; (c) Chen X.-t., Tong A.-j., *J. Lumin.,* **2014**, 145, 737-740; (d) Ma X., Cheng J., Liu J., Zhou X., Xiang H., *New J. Chem.,* **2015**, 39(1), 492-500.

[12] Cheng J., Li Y., Sun R., Liu J., Gou F., Zhou X., Xiang H., Liu J., *J. Mater. Chem. C,* **2015**, 3(42), 11099-11110.

[13] Ferguson L. N., Goodwin T. C., *J. Am. Chem. Soc.,* **1949**, 71(2), 633-637.

[14] Sinha U., *Acta Crystallogr., Sect. B: Struct. Crystallogr. Cryst. Chem.,* **1970**, 26(7), 889-895.

[15] Chen G. S., Anthamatten M., Barnes C. L., Glaser R., *J. Org. Chem.,* **1994**, 59(15), 4336-4340.

[16] Benson R. E., Roy T. G., Dey B. K., Barua K. K., Tiekink E. R., *Acta Crystallogr. Sect. Sect. E: Struct. Rep. Online,* **2006**, 62(5), o1971-o1972.

[17] Sauro V. A., Workentin M. S., *J. Org. Chem.,* **2001**, 66(3), 831-838.

[18] Tang X. D., Ding Z. J., Zhang Z. M., *Solid State Commun.,* **2009**, 149(7), 301-306.

[19] Baig F., Kant R., Gupta V. K., Sarkar M., *RSC Adv.,* **2015**, 5(63), 51220-51232.

[20] Kouznetsov V. V., Amado D. F., Bahsas A., Amaro-Luis J., *J. Heterocycl. Chem.,* **2006**, 43(2), 447-452.

[21] Khalkhali E., Nabipour H., *Inorg. Chem.: Indian J.,* **2012**, 7(2), 57-60.

[22] El-Qisairi A. K., Qaseer H. A., Alshahateet S. F., Qaseer M., Zaghal M. H., Al-Btoush W. e., Dawe L. N., *Croat. Chem. Acta,* **2014**, 87(2), 123-128.

[23] (a) Wang L., Shen Y., Yang M., Zhang X., Xu W., Zhu Q., Wu J., Tian Y., Zhou H., *Chem. Commun.,* **2014**, 50(63), 8723-8726; (b) Basak S., Nandi N., Baral A., Banerjee A., *Chem. Commun.,* **2015**, 51(4), 780-783.

[24] (a) Mitra A., Seaton P. J., Ali Assarpour R., Williamson T., *Tetrahedron,* **1998**, 54(51), 15489-15498; (b) LaPlante S. R., Carson R., Gillard J., Aubry N., Coulombe R., Bordeleau S., Bonneau P., Little M., O'Meara J., Beaulieu P. L., *J. Med. Chem.,* **2013**, 56(12), 5142-5150.